Site U1544

F. Lamy, G. Winckler, C.A. A Alvarez Zarikian, H.W. W Arz, C. Basak, A. Brombacher, O.M. M Esper, J.R. R Farmer, J. Gottschalk, L.C. C Herbert, et al.

Lamy, F., Winckler, G., Alvarez Zarikian, C.A., and the Expedition 383 Scientists
Proceedings of the International Ocean Discovery Program Volume 383
publications.iodp.org

https://doi.org/10.14379/iodp.proc.383.108.2021

Site U1544[1]

F. Lamy, G. Winckler, C.A. Alvarez Zarikian, H.W. Arz, C. Basak, A. Brombacher, O.M. Esper, J.R. Farmer, J. Gottschalk, L.C. Herbert, S. Iwasaki, V.J. Lawson, L. Lembke-Jene, L. Lo, E. Malinverno, E. Michel, J.L. Middleton, S. Moretti, C.M. Moy, A.C. Ravelo, C.R. Riesselman, M. Saavedra-Pellitero, I. Seo, R.K. Singh, R.A. Smith, A.L. Souza, J.S. Stoner, I.M. Venancio, S. Wan, X. Zhao, and N. Foucher McColl[2]

Keywords: International Ocean Discovery Program, IODP, *JOIDES Resolution*, Expedition 383, Dynamics of the Pacific Antarctic Circumpolar Current, Site U1544, Southern Ocean, South Pacific, Chilean margin, paleoceanography, Antarctic Circumpolar Current, oceanic fronts, Circumpolar Deep Water, Antarctic Intermediate Water, marine carbon cycle, dust, biological productivity, iron fertilization, southern westerly winds, Patagonian ice sheet, West Antarctic ice sheet

Contents

Background and objectives

Site U1544 (Proposed Site CHI-1C) is located on the upper continental slope of the southwest Chilean margin at 55°32.2′S, 71°35.6′W, at approximately 2090 m water depth and 32 nmi from the western entrance of the Beagle Channel in Tierra del Fuego (Figure **F1**). The site is situated upstream from the Drake Passage in the present-day pathway of the Cape Horn Current (CHC) and represents a northern branch of the Antarctic Circumpolar Current (ACC). Along with two previously drilled Expedition 383 sites, U1542 and U1543, this site completes a depth transect of drill sites that samples all major intermediate and deep water masses in the Southeast Pacific.

Tectonically, the southern Chilean margin is characterized by a complex geodynamic setting with oblique convergence between plates, transcurrent motion, and tectonic rotation on land (Polonia et al., 2007). The geodynamic setting is driven by relative movements between three main plates: Antarctica, Scotia, and South America. This complex setting results in a strong segmentation of the southern Chilean margin, which is clearly visible by bathymetric data and the available multichannel seismic (MCS) data (Polonia et al., 2007) (Figure **F2**). Two major fore-arc basins at ~53°–54.5°S and 55°–56.5°S are characterized by a thick sediment infill of up to ~3 km. Site U1544 is situated close to the axis of the southern fore arc basin on the continental crust of the Scotia plate. This southern basin most likely formed after the ridge consumption between 10 and 14 Ma. When accretion resumed, it contributed to an outer high that provided a barrier for the accumulation of continent-derived sediments. The upper unit in the southern basement, relevant for drilling, shows onlap terminations on both basin flanks.

Site U1544 lies on MCS Line IT95-181 ~3 nmi southeast of the intersection with Line IT95-171 (Figure **F3**) (Polonia et al., 2007). Sediments are mostly well stratified, and sediment cover at the site exceeds 2.5 km. Sediment echo sound (Parasound) profiles (Lamy, 2016) reveal poor to moderate penetration (~30 m) with distinct layering and an irregular surface, suggesting a succession of fine- to medium-grained sediments with occasional coarser grained composition.

Site U1544 is located underneath the southward flowing CHC, a northern branch of the ACC that continues toward the Drake Passage and provides a major fraction of the present-day northern Drake Passage transport (Well and Roether, 2003). Satellite-tracked surface drifters reveal that after crossing the East Pacific Rise, Subantarctic surface water of the ACC is transported northeastward across the Southeast Pacific toward the Chilean coast at ~45°S/75°W (Figures **F4**, **F5**, **F6**). Here, presently only a minor part of ACC water is deflected northward into the Humboldt Current System, whereas the major fraction is deviated southward toward the Drake Passage. The CHC thus transports a significant amount of northern ACC water toward the Drake Passage in a narrow ~100–150 km belt along the coast (Chaigneau and Pizarro, 2005). Modern surface current velocities within the CHC reach >35 cm/s, and high flow speeds of ~20 cm/s extend to middepths (Boisvert, 1969; Chaigneau and Pizarro, 2005).

[1] Lamy, F., Winckler, G., Alvarez Zarikian, C.A., Arz, H.W., Basak, C., Brombacher, A., Esper, O.M., Farmer, J.R., Gottschalk, J., Herbert, L.C., Iwasaki, S., Lawson, V.J., Lembke-Jene, L., Lo, L., Malinverno, E., Michel, E., Middleton, J.L., Moretti, S., Moy, C.M., Ravelo, A.C., Riesselman, C.R., Saavedra-Pellitero, M., Seo, I., Singh, R.K., Smith, R.A., Souza, A.L., Stoner, J.S., Venancio, I.M., Wan, S., Zhao, X., and Foucher McColl, N., 2021. Site U1544. *In* Lamy, F., Winckler, G., Alvarez Zarikian, C.A., and the Expedition 383 Scientists, *Dynamics of the Pacific Antarctic Circumpolar Current*. Proceedings of the International Ocean Discovery Program, 383: College Station, TX (International Ocean Discovery Program). https://doi.org/10.14379/iodp.proc.383.108.2021

[2] **Expedition 383 Scientists' affiliations.**

MS 383-108: Published 18 July 2021

Figure F1. Oceanographic and bathymetric setting, Site U1544. A. Overview map with marine geological features. Yellow lines = seismic lines available in the region. B. Detailed bathymetry with seismic lines and shotpoints.

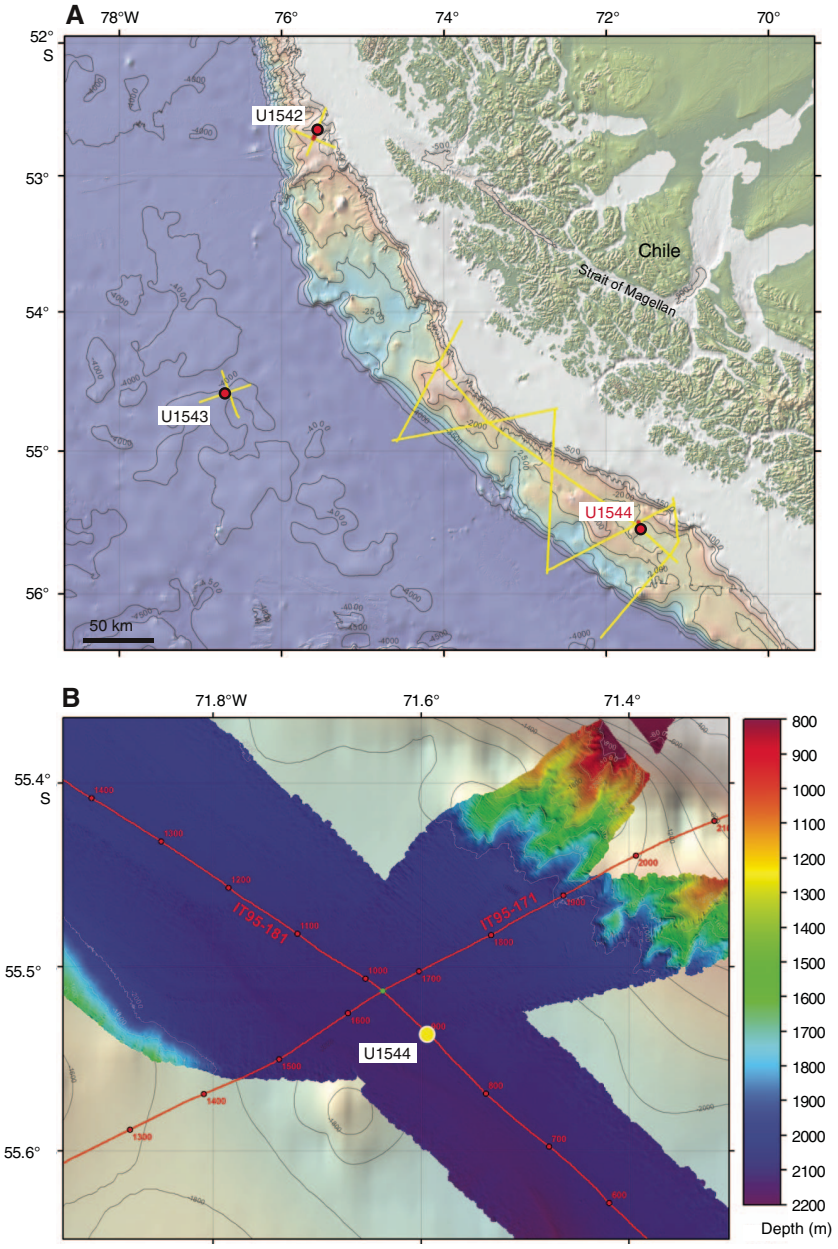

During R/V *Polarstern* Cruise PS97, several short cores were recovered in the fore-arc basin. They contained foraminiferal nannofossil ooze, the dominant lithology of Holocene sediments in the entire region (Lamy, 2016). Several piston and gravity coring attempts resulted in only relatively short cores with a maximum length of ~3 m (PS97–PS109) documenting a condensed, presumably Holocene section at the top and grading into glacial silty clay with occasional sandy layers and occasional ice-rafted debris that contain traces of plant material and indicate some admixture of shallow-water material (Lamy, 2016). In more condensed cores outside the fore-arc basin, calcareous sediments are confined to interglacials and suggest that foraminiferal ooze from the previous interglacial (Marine Isotope Stage 5) occurs at 6–10 m core depth, which was beyond the reach of conventional coring at proximal sites such as Site U1544.

Scientific objectives

The main objectives at Site U1544 were to

- Recover Pleistocene paleoceanographic records over the past several glacial–interglacial cycles with suborbital-scale resolution,
- Reconstruct the strength of the CHC (Subantarctic ACC) before entering the Drake Passage,
- Investigate Circumpolar Deep Water and Pacific Deep Water (PDW) mass properties,
- Investigate changes of continental paleoclimate, and
- Recover a potential near-field record of Patagonian ice sheet variability.

Figure F2. Large-scale geodynamic overview, Site U1544. The deep seismic record of Line IT95-171 is shown, along with the interpreted line drawing showing the tectonic units. Plots are after Polonia et al. (2007). s.p. = shotpoint, cdp = common depth point, BSR = bottom-simulating reflector.

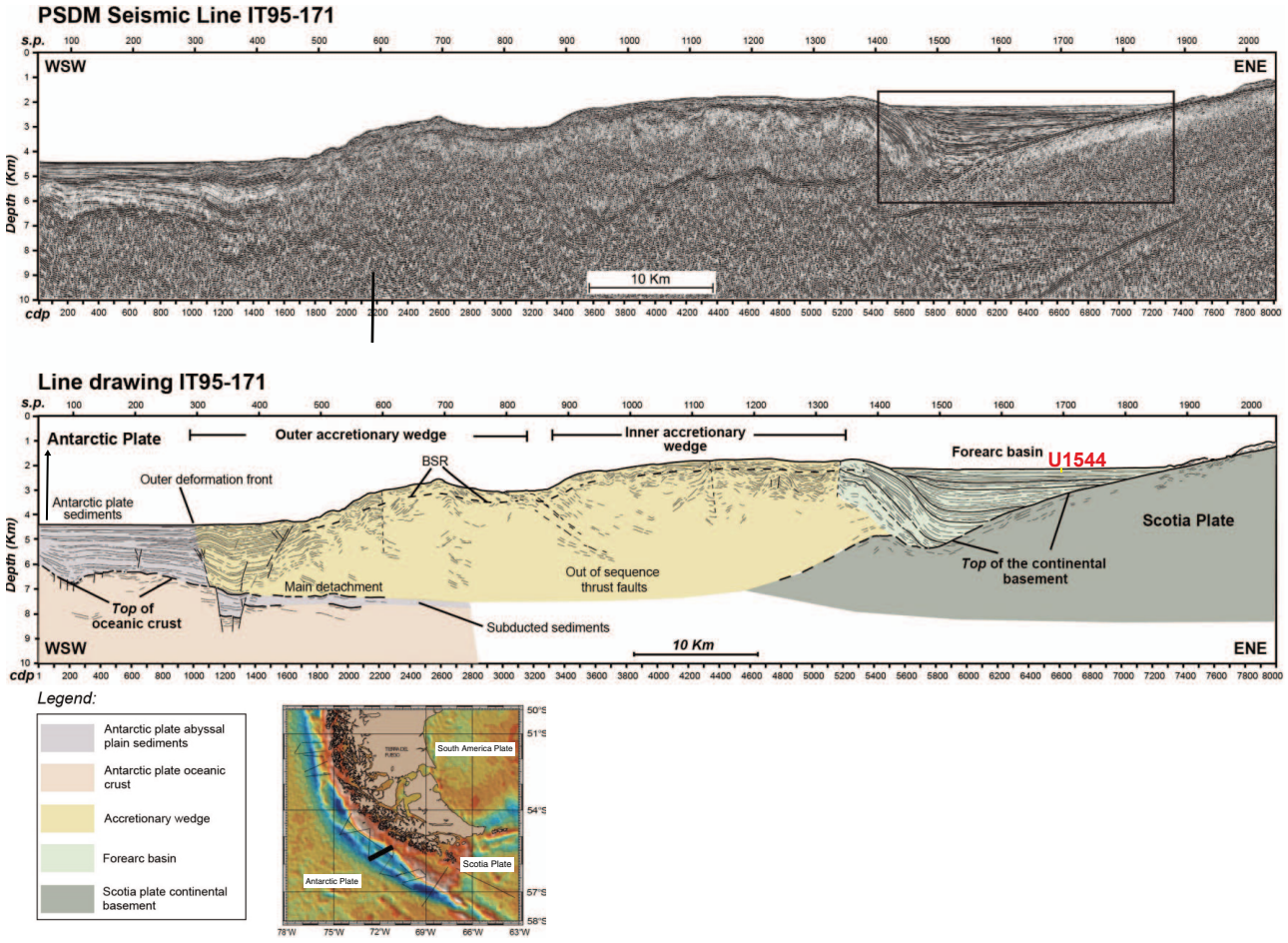

Figure F3. (Left) Multichannel seismic (MCS) and (Right) Parasound profiles across Site U1544. TWT = two-way traveltime.

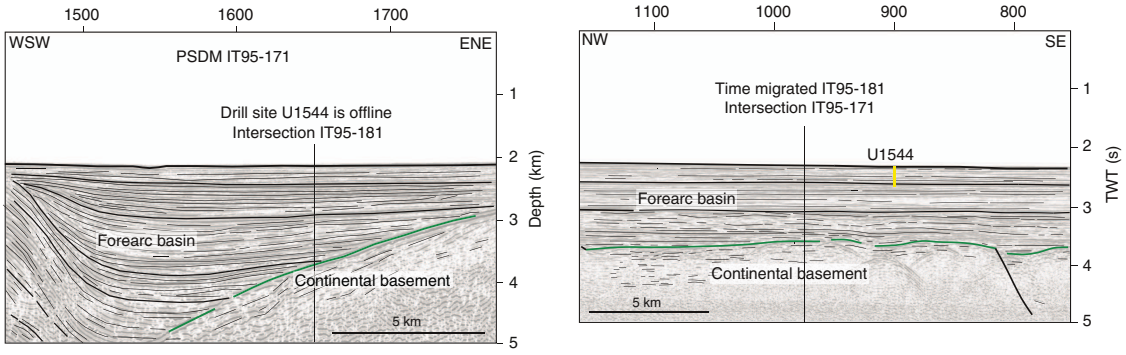

Figure F4. Surface circulation in the Southeast Pacific with examples of surface buoy trajectories (each 30-day position is marked by a circle) indicating northeast flow of northern Antarctic Circumpolar Current (ACC) water after crossing the East Pacific Rise. Also shown is the bifurcation of surface waters close to the Chilean coast (at about 45°S) with northward flowing water in the Humboldt Current System (HCS) and strongly accelerated southward flow in the Cape Horn Current (CHC) toward the Drake Passage. West–east drifting buoys follow the South Pacific Current (SPC). Modified from Chaigneau and Pizarro (2005) and Lamy et al. (2015).

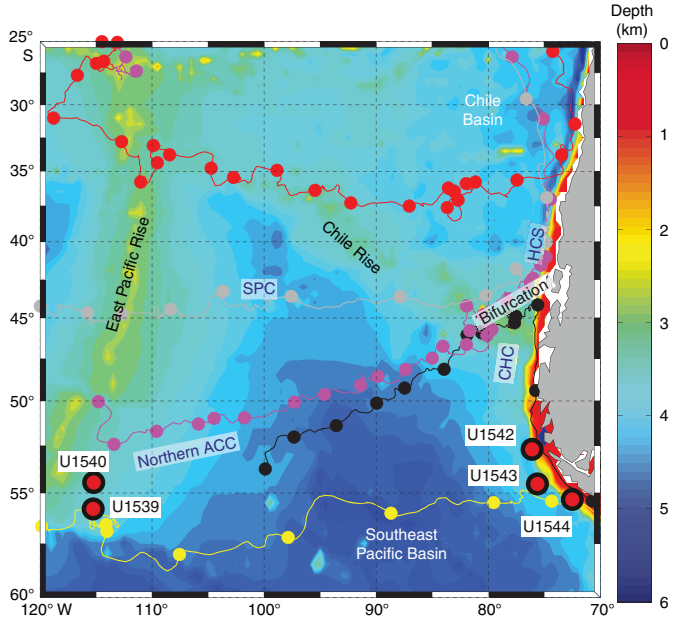

Figure F5. Schematic view of the southern Chilean margin and the Drake Passage region with major surface and intermediate water circulation and location of Expedition 383 sites and ODP Leg 202 Site 1233. HCS = Humboldt Current System, SPC = South Pacific Current, AAIW = Antarctic Intermediate Water, CHC = Cape Horn Current, ACC = Antarctic Circumpolar Current, SAF = Subantarctic Front, WSI = winter sea ice (approximate location).

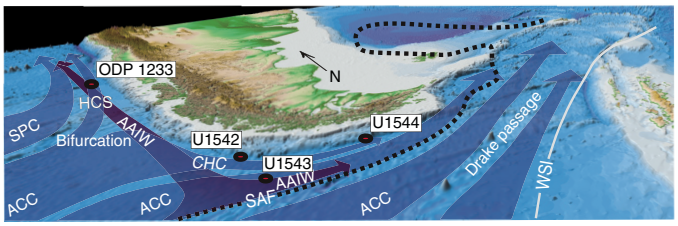

Figure F6. Modern oxygen distribution in the eastern South Pacific used to visualize major water masses. AAIW = Antarctic Intermediate Water, PDW = Pacific Deep Water, CDW = Circumpolar Deep Water, AABW = Antarctic Bottom Water.

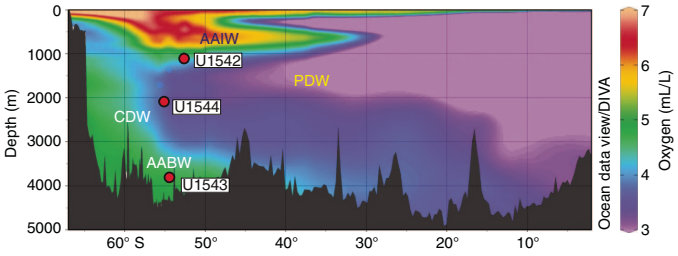

Operations

The initial plan for Site U1544 was to core three holes to 300 mbsf with core orientation and formation temperature measurements using the advanced piston corer temperature (APCT-3) tool in Hole U1544A. This plan was modified significantly because of time lost to weather during the expedition, shallowing the penetration depth to 50 mbsf. Orientation and temperature measurements were also dropped. Based on the weather forecast while coring Hole U1544A, we decided to deepen the first hole until advanced piston corer (APC) refusal and to abandon plans for the second and third holes. Ultimately, one hole was cored at this site using the extended core barrel (XCB) and APC systems over a 103 m interval. Core recovered was 91.34 m with 88.7% recovery.

Transit to Site U1544

The 184 nmi distance to Site U1544 was covered in 15.4 h at a speed of 12 kt. The R/V *JOIDES Resolution* arrived over the site coordinates at 1746 h on 14 July 2019. *JOIDES Resolution* then switched from cruising mode to full automatic dynamic positioning mode, and the rig crew started to assemble the APC/XCB bottom-hole assembly and deploy the drill string to the seafloor. By midnight, we had reached 2055 meters below rig floor (mbrf).

Site U1544

Hole U1544A

The initial attempt to spud Hole U1544A was made at 0015 h on 15 July 2019 and resulted in a bent/broken APC core barrel, which made it necessary to pull the bit back to the rig floor and remove the stuck portion of the barrel. The vessel was then moved 50 m southwest at 225° from the initial attempt for spudding. Because of a hard layer below the sediment surface, it was decided to use the XCB system to spud the hole and break through the layer.

Hole U1544A was finally spudded at 1330 h on 15 July with the XCB system advancing 7.8 m into a softer formation. The XCB barrel was then retrieved, and we found a ~5 cm size igneous rock in the core catcher. The full-length APC system was then deployed and used until refusal at 88.1 m core depth below seafloor, Method A (CSF-A). The half-length APC (HLAPC) system was then used to deepen the hole to the final depth of 106 m CSF-A before coring was terminated due to high seas and winds. The drill string was pulled out of the hole, clearing the seafloor at 0958 h on 16 July and ending Hole U1544A.

The vessel was offset 20 m of Hole U1544A with the bit at 2055 mbrf to wait for the seas to subside below 3.0 m of heave so that an attempt could be made to spud Hole U1544B. However, heave was still above 3.5 m at 0630 h on 17 July, and operations were terminated. Before pulling up the pipe, the core line was run to 1900 mbrf and then lubricated as it was pulled back on the winch. The coring assembly was broken down and stowed away, the drill string was recovered, and the rig floor was secured for transit. At 1330 h, *JOIDES Resolution* was under way to Punta Arenas, Chile.

A total of 19 cores were taken over a 103.0 m interval with 88.6% recovery. The XCB system was used once over a 4.8 m interval, retrieving 0.1 m. The APC system was then deployed 12 times over an 80.3 m interval, retrieving 73.48 m of sediment before refusal. The HLAPC was deployed for the final six cores of the site over a 17.9 m interval, recovering 17.70 m. All APC and HLAPC cores attempted at the site recorded partial strokes. A coring summary for Hole U1544A is shown in Table **T1**.

Table T1. Core summary, Site U1544. DRF = drilling depth below rig floor, DSF = drilling depth below seafloor, CSF = core depth below seafloor. APC = advanced piston corer, HLAPC = half-length APC, XCB = extended core barrel, RCB = rotary core barrel. Core type: H = APC, F = HLAPC, X = XCB, numeric = drilled interval. **Download table in CSV format.**

Hole: U1544A
Latitude: 55°32.2192′S
Longitude: 71°35.6194′W
Water depth (m): 2089.86
Date started (UTC, h): 14 Jul 2019 2045
Date finished (UTC, h): 16 Jul 2019 1300
Time on hole (days): 1.68
Seafloor depth DRF (m): 2101
Seafloor depth est. method: seafloor tag
Rig floor to sea level (m): 11.14
Penetration DSF (m): 106
Cored interval (m): 103
Recovered length (m): 91.34
Recovery (%): 88.68
Drilled interval (m): 3
Drilled interval (*N*): 1
Total cores (*N*): 19
APC cores (*N*): 12
HLAPC cores (*N*): 6
XCB cores (*N*): 1
RCB cores (*N*): 0
Other cores (*N*) 0

Core	Top depth drilled DSF (m)	Bottom depth drilled DSF (m)	Advanced (m)	Recovered length (m)	Curated length (m)	Top depth cored CSF (m)	Bottom depth recovered (m)	Recovery (%)	Date, time on deck (UTC h)	Sections (*N*)
383-U1544A-										
11	0.0	3.0	3.0	0.00	*****Drilled from 0.0 to 3.0 m DSF*****				15 Jul 2019 1530	0
2X	3.0	7.8	4.8	0.10	0.10	3.0	3.10	2	15 Jul 2019 1750	1
3H	7.8	17.3	9.5	9.59	9.59	7.8	17.39	101	15 Jul 2019 1845	8
4H	17.3	26.8	9.5	10.05	10.23	17.3	27.53	106	15 Jul 2019 1945	8
5H	26.8	36.3	9.5	9.58	9.61	26.8	36.41	101	15 Jul 2019 2040	9
6H	36.3	45.8	9.5	3.70	3.70	36.3	40.00	39	15 Jul 2019 2140	5
7H	45.8	55.3	9.5	7.56	7.63	45.8	53.43	80	15 Jul 2019 2230	7
8H	55.3	60.5	5.2	5.28	5.28	55.3	60.58	102	15 Jul 2019 2320	6
9H	60.5	68.5	8.0	8.08	8.04	60.5	68.54	101	16 Jul 2019 0045	7
10H	68.5	74.1	5.6	5.62	5.54	68.5	74.04	100	16 Jul 2019 0200	5
11H	74.1	78.7	4.6	4.61	4.61	74.1	78.71	100	16 Jul 2019 0305	4
12H	78.7	83.4	4.7	4.71	4.71	78.7	83.41	100	16 Jul 2019 0435	5
13H	83.4	84.7	1.3	1.35	1.35	83.4	84.75	104	16 Jul 2019 0535	2
14H	84.7	88.1	3.4	3.41	3.41	84.7	88.11	100	16 Jul 2019 0625	4
15F	88.1	90.2	2.1	2.09	2.09	88.1	90.19	100	16 Jul 2019 0730	3
16F	90.2	91.0	0.8	0.84	0.84	90.2	91.04	105	16 Jul 2019 0825	2
17F	91.0	94.5	3.5	3.56	3.56	91.0	94.56	102	16 Jul 2019 0915	4
18F	94.5	99.2	4.7	4.51	4.51	94.5	99.01	96	16 Jul 2019 1005	4
19F	99.2	101.9	2.7	2.54	2.54	99.2	101.74	94	16 Jul 2019 1100	3
20F	101.9	106.0	4.1	4.16	4.16	101.9	106.06	101	16 Jul 2019 1145	4

Approaching heavy weather and seas to the western entrance of the Strait of Magellan forced us to take the eastern route along the northern edge of the Drake Passage around Cape Horn and through Le Maire Strait. The 519 nmi from Site U1544 to Punta Arenas was completed at 1700 h on 19 July with the first line ashore at Pier 1 South, Prat Terminal, ending Expedition 383.

Sedimentology

Sediment cores from Hole U1544A were retrieved from a sedimentary infill sequence of a fore-arc basin that formed between the southwest Chilean continental margin and a topographically elevated accretionary wedge farther offshore. Given the difficulties obtaining a mudline at this site using the APC system because of an impenetrable surface layer (see **Operations**), recovered sediments do not cover the Holocene interval. A single ~5 cm clast of mafic intrusive igneous rock along with ~10 cm of silty clay was all that was recovered from an XCB core that penetrated the upper 10 m of the sedimentary sequence. Site U1544 sediments consist of siliciclastic material that mainly occurs as beds of silty clay and distinct sand layers with erosional basal contacts and normal grading. Biogenic components occur as a minor modifier of the terrigenous material with the exception of two distinct beds where calcareous biogenic sediments (foraminifers and nannofossils) dominate the sequence.

High heave during drilling operations due to rough seas caused core disturbances (i.e., fall-in at the top of sediment cores and suck-in at the base). The identification and classification of sediments disturbed by drilling operations is described in **Sedimentology** in the Expedition 383 methods chapter (Winckler et al., 2021) and is largely based on Jutzeler et al. (2014). Severe drilling-disturbed sediments were classified as mixed siliciclastic sediments in the visual core descriptions (VCDs) and hole summary (Figure **F7**). Given the distinct and frequent lithology changes between sand layers with a high water content and stiffer silty clay, vertical flowage of sediment

Figure F7. Hole summary, Hole U1544A. GRA = gamma ray attenuation, MSP = point magnetic susceptibility, RGB = red-green-blue, NGR = natural gamma radiation, cps = counts per second.

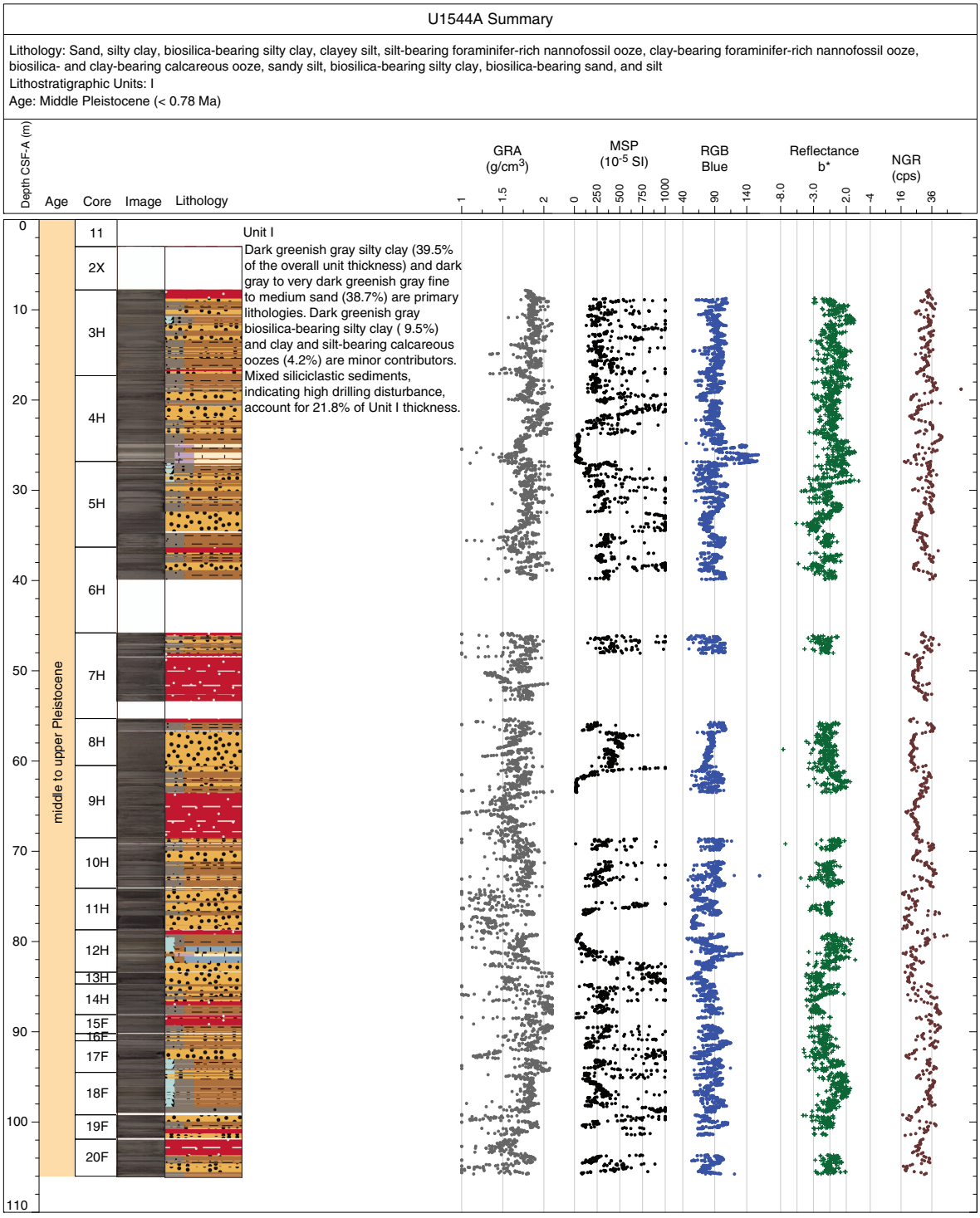

along the core liner, distortion of sediment boundaries, and uparching beds are frequently encountered at Site U1544. Examples of disturbed sediment due to drilling are found in Sections 383-U1544A-7H-2 through 7H-CC, 20F-1, and 20F-2.

Lithofacies description

Four lithofacies were identified at Site U1544 (Table **T2**). The two dominant siliciclastic lithofacies can be represented in a ternary diagram with sand, silt, and clay as the main components, and the remaining lithofacies with biogenic contributions can be represented in a ternary diagram with carbonates, biogenic silica, and combined clay and silt as the main components (Figure **F8**). The numbering of the facies is based on the cumulative lithofacies documented for all Expedition 383 sites, but only lithofacies documented at Site U1544 are described and discussed here.

Table T2. Description of lithofacies, Site U1544. **Download table in CSV format.**

Type	Lithofacies	Description	Thickness (m)	Degree of bioturbation	Color	Proportion in Lith. Unit I (%)	Depositional environment
Biosilica-bearing silty clay	7	Biosilica- and silt-rich clay; undifferentiated broken biosiliceous debris; occasionally mottled	0.1–1.4	Slight-heavy	Greenish gray (10Y 5/1) to dark greenish gray (10Y 4/1)	9.5	Hemipelagic
Silty clay	8	Silty clay with rare to trace occurrences of biogenic components (including diatoms, radiolarians, sponge spicules, and silicoflagellates) and sand; frequently mottled; occasionally intercalated with millimeter-scale silt layers	0.02–2.0	Slight-heavy	Greenish gray (10Y 5/1) to dark greenish gray (10Y 4/1)	39.5	Hemipelagic
Siliciclastic-bearing to -rich nannofossil or calcareous ooze	10	Biosilica-, silt-, and clay-bearing to silty calcareous ooze or slit-, clay-, and/or foraminifer-bearing to -rich nannofossil ooze; heavily bioturbated; massive appearance	0.6–1.2	Heavy	Light gray (N 7/0) to dark greenish gray (10Y 4/1)	4.2	Hemipelagic
Sand	11	Fine to medium sand containing mafic (mica and hornblende) and felsic (mostly quartz) minerals, calcareous (shell) debris, and foraminifers; subangular to angular grains, moderately sorted	0.02–3.8	Slight	Very dark greenish gray (10Y 3/1) to black (N 2.5/0)	38.7	Hemipelagic

Lithofacies 8 and 11 dominate the Site U1544 sedimentary sequence. They transition from silt-bearing clay to clay-bearing silt with only trace biosiliceous components (Lithofacies 8) to a fine to medium sand with trace foraminifers and other biosiliceous and siliciclastic components (Lithofacies 11). The principal lithologies with biogenic components are biosilica-bearing clay to silt (Lithofacies 7) and calcareous ooze with minor to major modifier abundances of foraminifers, silt, clay, and biosilica (Lithofacies 10).

Lithofacies 7

Lithofacies 7 is greenish gray (10Y 5/1) to dark greenish gray (10Y 4/1) biosilica-bearing silty clay (Figure **F9**). Biosiliceous debris is undifferentiated and may include diatoms, radiolarians, and sponge spicule fragments. The bed thickness of Lithofacies 7 varies from 0.1 to 1.4 m, and bioturbation is slight to heavy. Representative examples are found in Sections 383-U1544A-3H-3, 5H-1, 5H-2, and 18F-1 through 18F-3.

Lithofacies 8

Lithofacies 8 is greenish gray (10Y 5/1) to dark greenish gray (10Y 4/1) silty clay with rare to trace sand and biosiliceous components (diatoms, radiolarians, sponge spicules, and silicoflagellates) (Figure **F10**). This lithofacies is slightly to heavily bioturbated and often contains dark gray mottling (N 4/0) The thickness of this lithofacies in the sedimentary record varies from 0.02 to 2 m, and representative examples are found in Sections 383-U1544A-3H-4, 10H-3, and 20F-2.

Lithofacies 10

Lithofacies 10 is a light gray (N 7/0) to dark greenish gray to greenish gray (10Y 4/1) calcareous ooze that contains a significant proportion of siliciclastic material (mainly clay and silt), foraminifers, and biogenic silica. At Site U1544, it appears in the form of heavily bioturbated, massively bedded silt- or clay-bearing foraminifer-rich nannofossil ooze or biosilica- and clay-bearing calcareous ooze (Figure **F11**). The bed thickness of Lithofacies 10 varies from 0.6 to 1.2 m. This lithofacies is only found in Sections 383-U1544A-4H-6, 4H-7, 12H-2, and 12H-3.

Lithofacies 11

Lithofacies 11 is very dark greenish gray (10Y 3/1) to black (N 2.5/0) fine to medium, subangular to angular, moderately sorted sand (Figure **F12**). This sand is principally composed of quartz, feldspar, and mafic minerals like hornblende, pyroxene, and mica and has accessory components of calcareous (shell) debris and foraminifers. Basal contacts with underlying lithofacies are sharp and erosive (Figure **F13**). Individual occurrences exhibit normal grading and vary in thickness from 0.02 to 3.8 m.

Lithostratigraphic units

The Site U1544 sedimentary sequence comprises one lithostratigraphic unit (Figure **F14**). Key unit characteristics, including depths within the Site U1544 sedimentary sequence and corresponding ages according to the preliminary shipboard age model, are described below.

Unit I

Interval: 383-U1544A-2X-CC, 0 cm, to 20F-3, 25 cm
Depth: 7.7–106.1 m CSF-A
Thickness: 98.4 m
Age: middle and upper Pleistocene (younger than 0.42 Ma)
Lithology: sand, silty clay, biosilica-bearing silty clay, clayey silt, silt-bearing foraminifer-rich nannofossil ooze, clay-bearing foraminifer-rich nannofossil ooze, biosilica- and clay-bearing calcareous ooze, sandy silt, biosilica-bearing silty clay, biosilica-bearing sand, and silt

Lithostratigraphic Unit I spans the entirety of the Hole U1544A sedimentary sequence (Figure **F14**) and largely consists of dark greenish gray silty clay (Lithofacies 8; 39.5% of the overall unit thickness) and dark gray to very dark greenish gray fine to medium sand (Lithofacies 11; 38.7%) (Figures **F7**, **F15**). Dark greenish gray biosilica-bearing silty clay (Lithofacies 7; 9.5%) and clay- and silt-bearing calcareous oozes (Lithofacies 10; 4.2%) are minor contributions. Mixed siliciclastic sediments that indicate high drilling disturbance account for 21.8% of the overall thickness. Bioturbation ranges from slight to heavy, and except in the uppermost part, dropstones are

Figure F8. Lithofacies observed at Site U1544 (and other Expedition 383 sites) in (A) siliciclastic and (B) combined siliciclastic-biogenic ternary sedimentary diagrams that include (A) silt, sand, and clay and (B) carbonates, diatoms, and combined silt and clays as defining components.

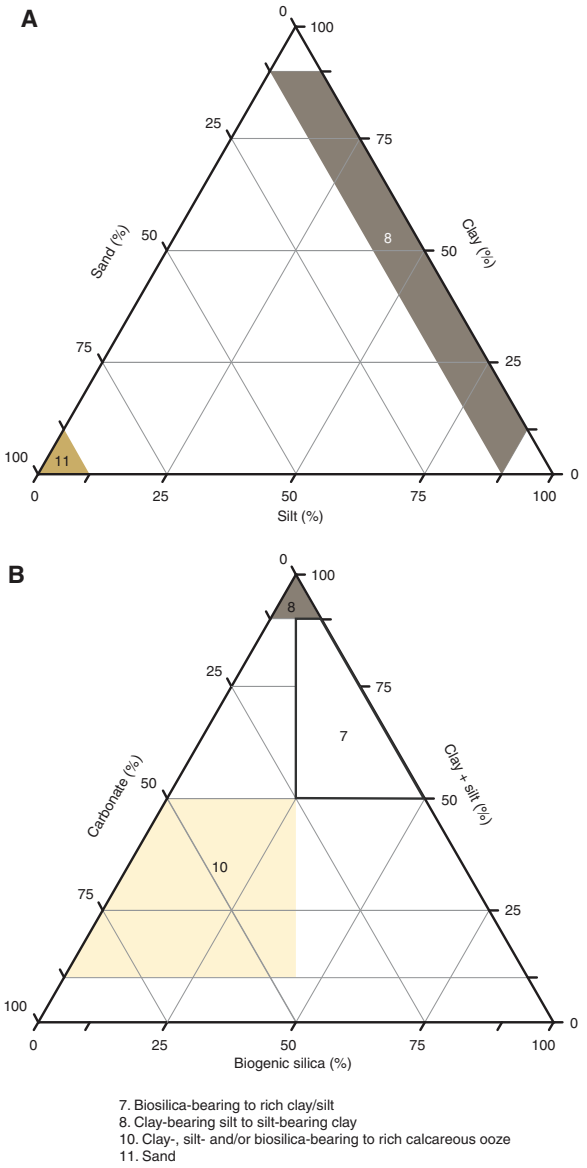

Figure F9. Representative (A) core and (B) X-ray and photomicrograph images of mineral properties of Lithofacies 7 (biosilica-bearing silty clay) in (C) plane-polarized light (PPL) and (D) cross-polarized light (XPL), Site U1544.

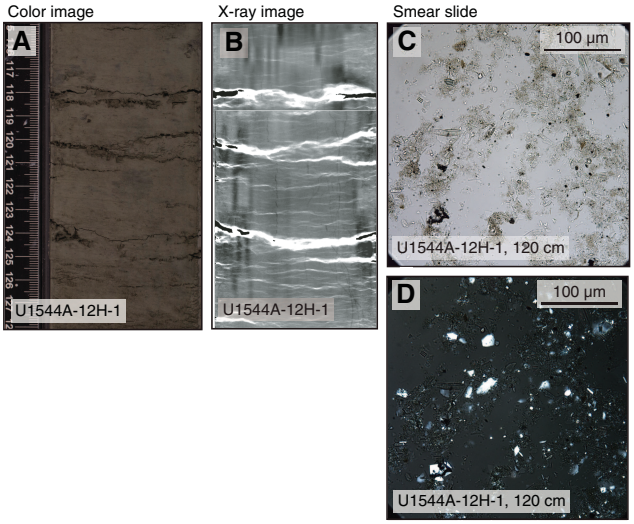

Figure F10. Representative (A) core and (B) X-ray and photomicrograph images of mineral properties of Lithofacies 8 (silty clay) in (C) PPL and (D) XPL, Site U1544.

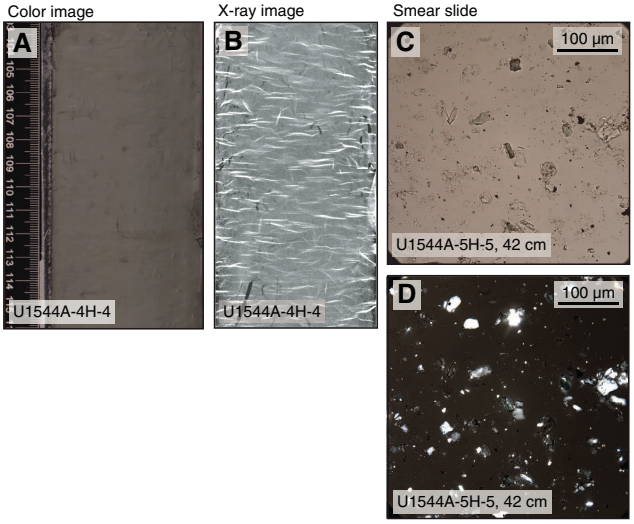

not observed in the split sediment core surface and are infrequently visible in X-ray images.

Complementary analyses

Integrating physical property measurements with lithofacies observations

The distribution of Site U1544 lithologies was compared to downcore physical property measurements including gamma ray attenuation (GRA) bulk density, natural gamma radiation (NGR), magnetic susceptibility (MS), red-green-blue color space (RGB) blue intensity, and color reflectance b* (see **Physical Properties** in the Expedition 383 methods chapter (Winckler et al., 2021) to identify principal relationships between lithologic observations and the physical properties of the sediment (Figure **F16**). Intervals dominated by sand (Lithofacies 11) are generally characterized by higher GRA bulk density, lower NGR, and lower RGB blue intensity values, whereas biosilica-bearing silty clay and silty clay (Lithofacies 7 and 8) are generally characterized by somewhat lower GRA bulk density and higher NGR and RGB blue intensity values. Conversely, intervals dominated by nannofossil ooze (Lithofacies 4 and 10) are generally characterized by lower GRA bulk density values, lower MS, lower NGR intensity, higher RGB blue intensity values, and higher color reflectance b*, consistent with observations at previous Expedition 383 sites.

Because Site U1544 operations occurred under time constraints, insufficient shipboard bulk sedimentary carbonate analyses were obtained to compare with physical property data (see **Geochemistry**), as was done at previous Expedition 383 sites. A comparison of physical property data sets with sediment carbonate content will have to occur after the expedition.

Figure F11. Representative (A) core and (B) X-ray and photomicrograph images of mineral properties of Lithofacies 10 (clay-, silt- and/or diatom-bearing to -rich calcareous ooze) in (C) PPL and (D) XPL, Site U1544.

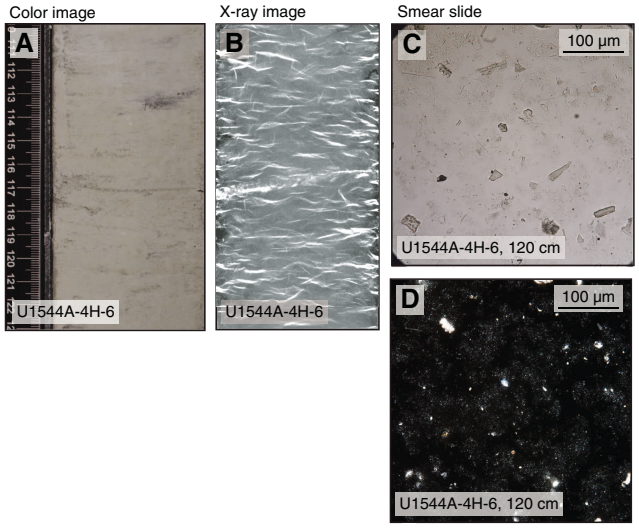

Figure F12. Representative (A) core and (B) X-ray and photomicrograph images of mineral properties of Lithofacies 11 (sand) in (C) PPL and (D) XPL, Site U1544.

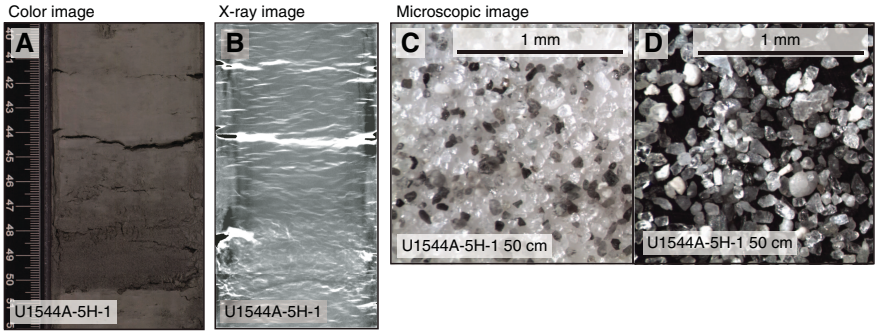

Figure F13. Erosive basal contacts of Lithofacies 11 with surrounding lithofacies, Site U1544.

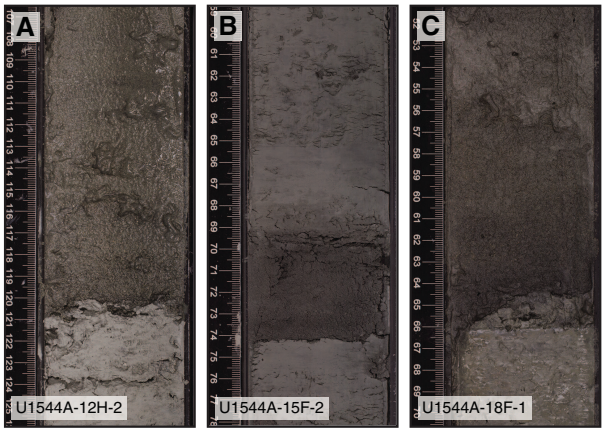

Summary and preliminary site interpretation

The sedimentary sequence at Site U1544 is characterized by one lithostratigraphic unit, Unit I (7.7–106.1 m CSF-A), which is dominated by siliciclastic sediments (i.e., silt and clay) that are frequently interbedded with sand layers and rare biogenic (i.e., nannofossil) oozes (Figures **F7**, **F14**). Although the dominant lithology at Site U1544 (silty clay) contains a minor or accessory contribution of biosilica and sand, the recurrent beds of sands that show erosional bases and normal grading are nearly entirely composed of subangular to angular, moderately sand-sized quartz and other minerals. The rare occurrence of nannofossil ooze at 26–28 and 80.5–82.5 m CSF-A is linked with positive excursions in color reflectance L* and

Figure F14. Summary of primary lithostratigraphic variations, Site U1544. MSP = point magnetic susceptibility, RGB = red-green-blue.

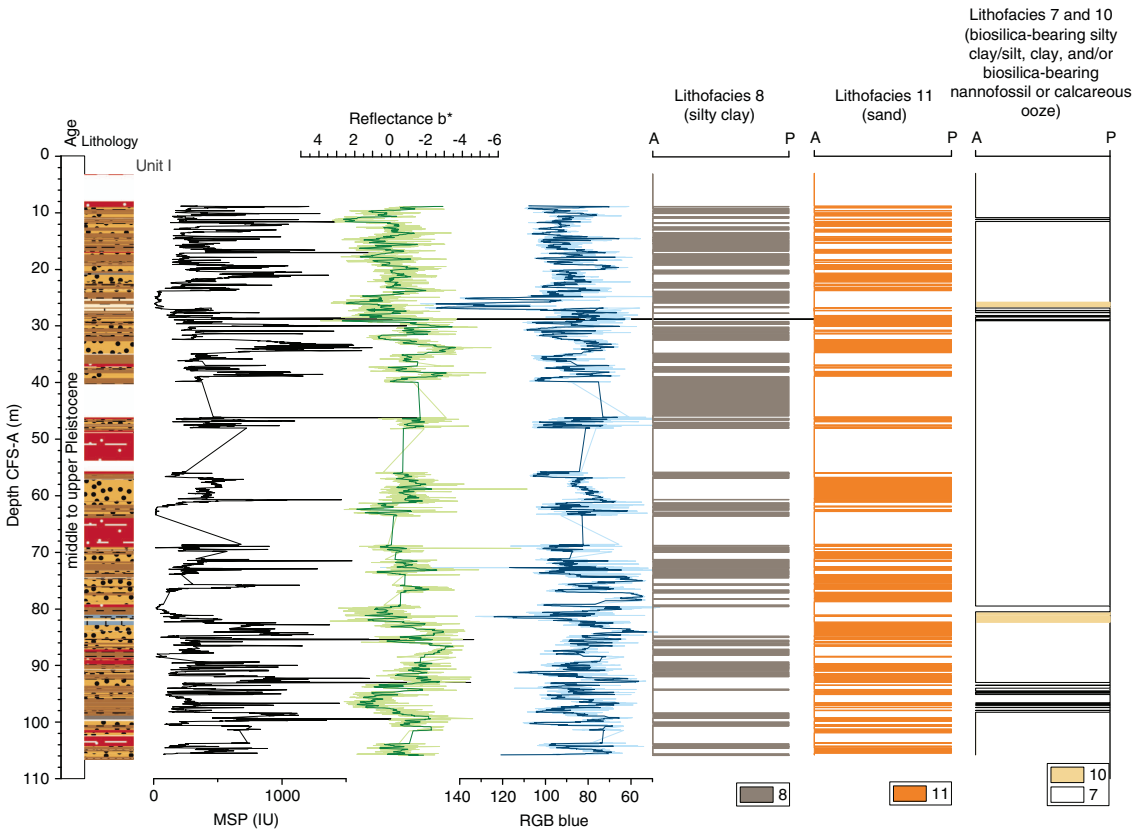

Figure F15. Relative contribution of lithofacies to Lithostratigraphic Unit I, Site U1544.

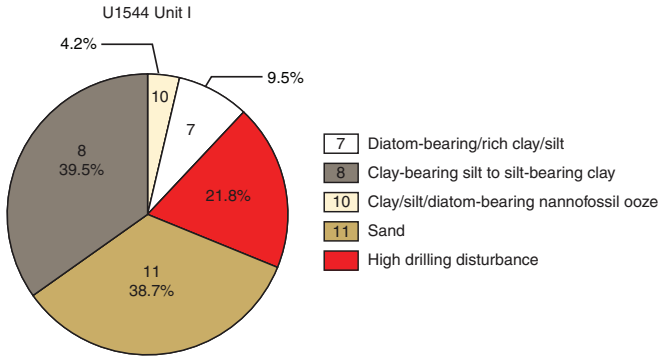

RGB blue intensity that also parallel reductions in MS and NGR. Most of the sediment sequence at Site U1544, however, is characterized by alternations between clay (Lithofacies 7 and 8) and sand beds (Lithofacies 11) that are clearly reflected in the physical property data. Prominent beds of greenish gray to dark greenish gray silty clay or biosilica-bearing silty clay coincide with higher b* values and lower MS, whereas sand layers show the opposite (Figure **F16**).

The close proximity of Site U1544 to the southernmost Chilean margin explains the dominance of terrigenous sediments at this site. Terrigenous sediment is likely delivered to the site by a combination of ice rafting, suspension fall-out from glacial meltwater plumes and/or freshwater plumes that originate from nonglaciated catchments, episodic downslope transport from the outer continental shelf, and fine-grained sediments transported by the CHC entering the Drake Passage as a northern branch of the ACC (Lamy et al., 2015). The large proportion of normally graded sand beds that have erosive basal contacts with the underlying silty clay lithologies implies that turbidity currents were a transport mechanism to carry sediments from the continental slope and the upper slope during the middle and late Pleistocene. We conservatively estimate the contribution of turbidite deposits as ~40% based on the thickness of sand layers (Lithofacies 11). However, it is possible that a certain fraction of the hemipelagic sediments also represents a continuation of the normal graded turbidite deposition sequence. If so, turbidites may account for a larger proportion of the sequence, implying that sedimentation at Site U1544 was rather discontinuous. In contrast, sedimentation during interglacials (the rare biogenic oozes) is unaffected by sediment redeposition and rather undisturbed. Future geochemical and sedimentary analyses will provide needed insights into the nature and temporal evolution of sedimentation processes at Site U1544.

Figure F16. Characteristic variations in major lithology and physical properties, Hole U1544A. Horizontal brown bars = sand (Lithofacies 11), light brown bars = nannofossil ooze (Lithofacies 4 and 10; pale orange), white bars = siliciclastic sediments, typically silty clay (Lithofacies 7 and 8). GRA = gamma ray attenuation, NGR = natural gamma radiation, cps = counts per second, MS = point magnetic susceptibility, RGB = red-green-blue.

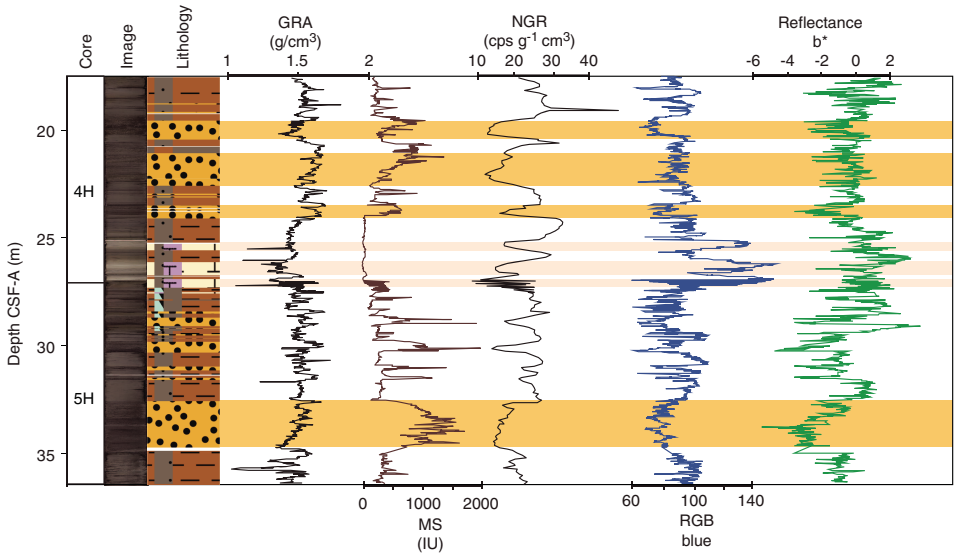

Biostratigraphy

Core catcher samples from Site U1544 were analyzed for siliceous (diatoms, radiolarians, and silicoflagellates) and calcareous (nannofossils, foraminifers, and ostracods) microfossils. Microfossil occurrence and abundance is variable at Site U1544. Diatoms are barren to abundant throughout the succession, and they show moderate to high dissolution and moderate to high fragmentation. Radiolarians are rare and poorly preserved in the majority of the samples examined from Site U1544. Silicoflagellates are not present throughout the sediment sequence. Calcareous nannofossils are rare to abundant, and preservation is generally poor to moderate throughout the sequence. Planktonic and benthic foraminifers are abundant above ~85 m CSF-A, and preservation is generally moderate to good. Planktonic and benthic foraminifers are rare below ~85 m CSF-A because of dilution by the very high silt and clay content.

The biostratigraphy at Site U1544 is not well constrained because of the absence of marker species for most of the fossil groups; however, the constraints available indicate a middle to late Pleistocene age for the recovered sequence (Table **T3**). Diatom assemblages provide one biostratigraphic datum, and the absence of another species throughout the record provides an indirect constraint, suggesting an age younger than 0.42 Ma at the bottom of Hole U1544A. Calcareous nannofossil ages are not accurately constrained because of poor preservation of marker species in samples deeper than Sample 383-U1544A-5H-CC. No radiolarian or planktonic foraminifer marker fossils were found at this site. Abundances of the different microfossil groups in Hole U1544A are shown in Figure **F17**.

Diatoms

Diatom biostratigraphy at Site U1544 is based on the analysis of 24 smear slides from 19 core catcher samples and 5 working-half samples from Hole U1544A. Diatom abundances vary from barren to abundant; in total, three smear slides were barren of diatoms due to high dilution by terrigenous clay, silt, and sand (Figure **F17**). Dissolution is high to moderate, and most samples exhibit high to moderate fragmentation (Table **T4**).

The diatom assemblage compositions in Hole U1544A are internally consistent, and the datums agree fairly well with the Pleistocene to recent sequence at Site U1539. The diatom succession appears to record continuous accumulation from the recent to the middle Pleistocene, following the diatom zonation of Zielinski and Gersonde (2002), with a basal age younger than 0.42 Ma in Hole U1544A (Table **T4**; Figure **F18**). Besides diatoms, few to common sponge spicules and traces of organic-walled dinoflagellate cysts (dinocysts) were noted.

The diatom assemblages in Hole U1544A reflect the upper part of the *Thalassiosira lentiginosa* Partial Range Zone and are characterized by the sporadic appearance of common to rare *T. lentiginosa* and few to rare *Azpeitia tabularis*, *Eucampia antarctica*, and *Fragilariopsis kerguelensis*. The boundary between Subzones C and B, marked by the last occurrence of *Hemidiscus karstenii*, was identified in Sample 383-U1544A-8H-CC (60.52–60.58 m CSF-A). Subzones B and A of the *T. lentiginosa* Zone, divided by the first Quaternary common occurrence of *H. karstenii*, are undifferentiated in Hole U1544A. *Actinocyclus ingens*, whose last appearance datum of 0.42 Ma provides an alternate constraint for the Subzone B/A boundary, was not identified in any samples from Site U1544, constraining the basal age of Hole U1544A to younger than 0.42 Ma.

Radiolarians

Eighteen core catcher samples from Hole U1544A were processed and analyzed for radiolarian assemblages (Samples 383-U1544A-3H-CC through 20F-CC; 17.33–106.06 m CSF-A). A total of 16 species were identified, and their distribution is documented in Table **T5**. Radiolarians are rare in most samples from Hole U1544A and absent in Samples 7H-CC (53.28 m CSF-A), 11H-CC (78.65 m CSF-A), and 18F-CC (98.95 m CSF-A) (Figure **F17**). Preservation is moderate in the top part of Hole U1544A (17.33–27.47 m CSF-A) and deteriorates to poor downhole. Because of the scarcity of radiolarians and poor preservation at Site U1544, no biostratigraphic events were documented.

Table T3. Chronostratigraphic constraints at Site U1544. Event datum type: D = diatom, N = calcareous nannofossil. FO = first occurrence, LO = last occurrence. * = datums applied with lower confidence based on preservation, age, or depth uncertainty. — = not applicable. References: AO = Anthonissen and Ogg (2012), HM = Harwood and Maruyama (1992), ZG = Zielinski and Gersonde (2002). **Download table in CSV format.**

Constraint number	Type	Bioevent	Age (Ma)	Top core, section, interval (cm)	Top depth CSF–A (m)	Bottom core, section, interval (cm)	Bottom depth CSF–A (m)	Reference
				383-U1544A-		383-U1544A-		
1	N	FO *Emiliania huxleyi**	0.29	5H-CC, 5–11	36.35–36.41	6H-CC, 0–8	39.92–39.98	AO
2	D	LO *Hemidiscus karstenii*	0.19	7H-CC, 8–14	53.37–53.43	8H-CC, 7–13	60.52–60.58	HM, ZG
3	D	absence *Actinocyclus ingens**	<0.42	20F-CC, 19–25	106.00–106.06	Maximum age at base of core	—	ZG

Figure F17. Distribution of siliceous and calcareous microfossils, Hole U1544A. B = barren, R = rare, F = few, C = common, A = abundant, D = dominant. Ostracods reported as number of valves per sample (>125 mm fraction).

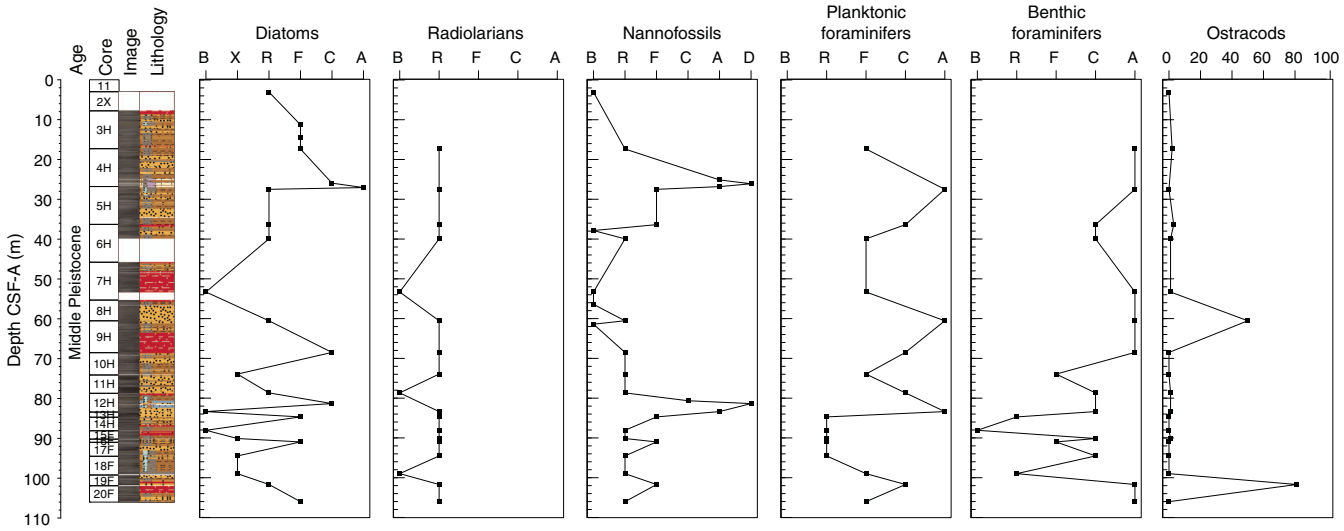

Table T4. Distribution chart of diatoms, Hole U1544A. **Download table in CSV format.**

Silicoflagellates

Silicoflagellates are not present at Site U1544.

Calcareous nannofossils

The calcareous nannofossil biostratigraphy is based on the analysis of 27 samples: 19 core catcher and 8 working-half toothpick samples from Hole U1544A (3.99–106.06 m CSF-A). Nannofossils are mostly absent or present in low abundance, generally rare to few, throughout the sequence (Figure **F17**; Table **T6**). However, they occasionally become abundant or dominant in specific intervals (i.e., Samples 383-U1544A-4H-6, 17 cm, to 4H-7, 31 cm [25.14–26.82 m CSF-A], and Samples 12H-2, 126 cm, and 13H-CC [80.65–84.75 m CSF-A]) that correspond to nannofossil oozes dominated by *Emiliania huxleyi* and *Gephyrocapsa* (<4 µm), respectively. The preservation of calcareous nannofossils is broadly poor to moderate at Site U1544, and it is only good in Samples 4H-6, 17 cm, to 4H-6, 113 cm (25.14–26.10 m CSF-A). The nannofossil assemblage at Site U1544 consists of 11 groups/taxa including *E. huxleyi, Gephyrocapsa margerelii/muellerae, Gephyrocapsa caribbeanica, Gephyrocapsa oceanica, Gephyrocapsa* spp. (<4 µm) small, *Coccolithus pelagicus, Calcidiscus leptoporus, Helicosphaera carteri, Syracosphaera* spp. (including *Syracosphaera pulchra*), and *Umbilicosphaera* spp. Reworked species were rarely found in Sample 3H-CC (Table **T6**). No biostratigraphic events were observed at Site U1544; however, the presence of *E. huxleyi* in Samples 3H-CC (17.33–17.39 m CSF-A) through 5H-CC (39.92–39.98 m CSF-A) suggests nannofossil Zone CN15/NN21 for this interval. It was not possible to accurately constrain the first occurrence of *E. huxleyi* because of poor coccolith preservation observed in samples deeper than Sample 5H-CC.

Foraminifers

Planktonic foraminifers

A total of 18 core catcher samples from Hole U1544A were analyzed for planktonic foraminifers (Table **T7**). Planktonic foraminifers are abundant in most samples in the upper 84 m of Hole U1544A, but abundance decreases in Samples 383-U1544A-13H-CC through 17F-CC (84.69–9594.56 m CSF-A). Preservation is generally moderate to good. Assemblages in Hole U1544A are characterized by both high-latitude and temperate species. *Neogloboquadrina pachyderma* (sinistral) dominates the assemblages throughout the record, and *Globigerina bulloides* is present throughout the sequence. Other species that occur in lower abundances are *Truncorotalia crassaformis, Truncorotalia truncatulinoides, Globoconella inflata, Turborotalita quinqueloba, Globigerinita glutinata, Globigerinita uvula, Orbulina universa, Neogloboquadrina incompta*, and *Hirsutella scitula*. Examples of key planktonic foraminifers found at Site U1544 are shown in Figure **F19**.

Figure F18. Diatom and calcareous nannofossil zonations and biostratigraphic events, Hole U1544A.

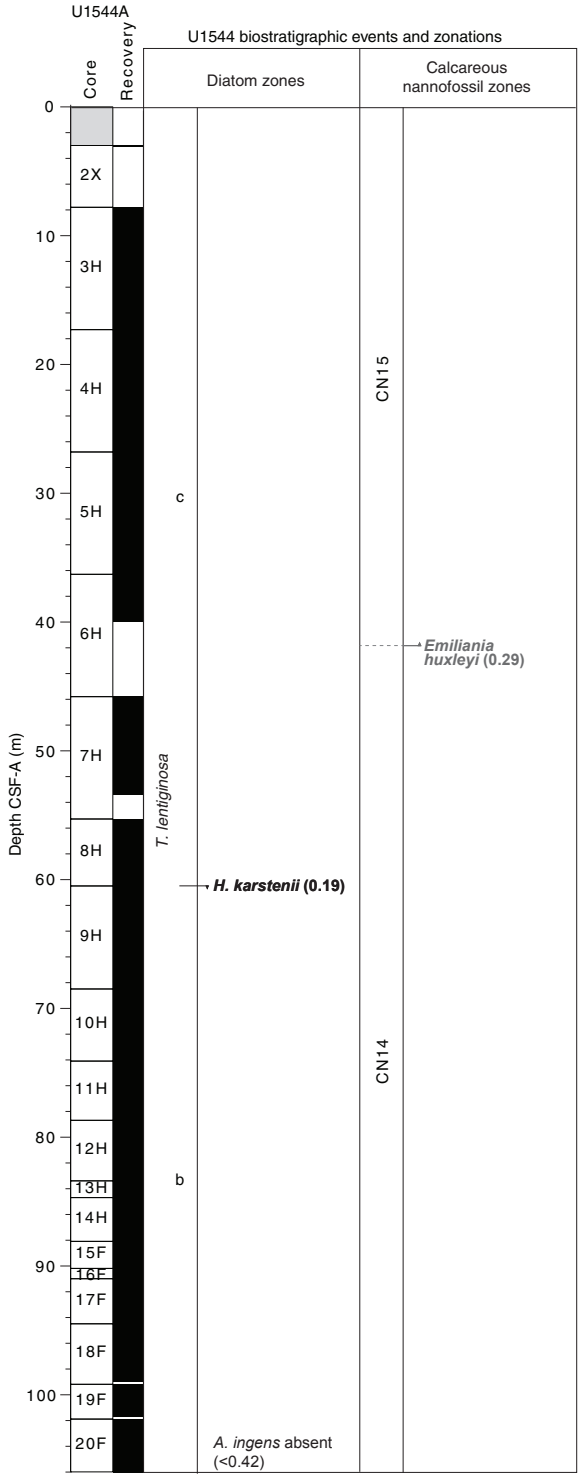

Planktonic foraminiferal assemblages at Site U1544 are typical of the Holocene–Pleistocene interval. *T. truncatulinoides* was found only in Sample 383-U1544A-4H-CC (27.47–27.53 m CSF-A), which indicates Zone SN14 of Jenkins (1993). *G. inflata* was observed in all core catcher samples from Hole U1544A, indicating that the bottom of the hole is younger than 3.13 Ma. *T. crassaformis* is present in the majority of core catchers between Samples 6H-CC and 20F-CC (39.92–106.06 m CSF-A), suggesting that this interval is younger than 4.5 Ma. One specimen of *Globorotalia puncticulata puncticuloides* was found in Sample 19F-CC, which suggests an age of ~0.7 Ma (Hornibrook, 1981; Hornibrook and Jenkins, 1994; Wei, 1994; Scott et al., 2007). However, this age does not agree with the diatom age estimate of younger than 0.42 Ma for the same sample. Given the presence of turbidites in Core 19F and no other records of *G. puncticulata puncticuloides* in Cores 19F and 20F, this specimen was probably reworked, and it has been discarded from the biostratigraphy.

Table T5. Distribution chart of radiolarians, Hole U1544A. **Download table in CSV format.**

Table T6. Distribution chart of calcareous nannofossils, Hole U1544A. **Download table in CSV format.**

Table T7. Distribution chart of planktonic foraminifers, Hole U1544A. **Download table in CSV format.**

Benthic foraminifers

Benthic foraminifers were examined in 18 core catcher samples from Hole U1544A. Specimens were picked from both the >125 µm fraction and the 125–63 µm fraction to ensure that assemblages in the >125 µm fraction were representative and that small species such as phytodetritus feeders or small infaunal taxa were not overlooked.

Benthic foraminifers at this site are moderately to well preserved (Figure **F17**; Table **T8**). Samples 383-U1544A-13H-CC through 18F-CC are dominated by clay and silt. Hence, very little coarse fraction residue remained after washing over 63 µm sieves, particularly for Samples 14H-CC and 18F-CC.

In total, 62 benthic foraminiferal taxa were identified at this site. Table **T8** summarizes the downcore distribution of benthic foraminifers in core catcher samples from Hole U1544A, some of which are also shown in Figure **F20**. The characteristic taxa found at this site were the same as those found at central South Pacific Sites U1539–U1541 and at Chilean margin Site U1542. The overall assemblage composition indicates that bathyal paleodepths and shelf fauna are mixed into Samples 383-U1544A-7H-CC, 10H-CC, 16F-CC, and 19F-CC. Species commonly recorded through the sequence include the calcareous species *Cibicides/Cibicidoides* spp., *Ehrenbergina* sp., *Fursenkoina complanata, Globocassidulina subglobosa, Melonis barleeanum, Oridorsalis umbonatus*, and *Uvigerina peregrina* (Figure **F20**). *Nuttallides umbonifera*, a species indicative of corrosive bottom water (Singh and Gupta, 2010; Bremer and Lohmann, 1982), appears in sporadic occurrences and peaks below 85 m CSF-A. *Cassidulina laevigata*, a species typical of shelf areas (Murray, 1991) and associated with relatively cold water (Fontanier et al., 2003), has peak occurrences in Samples 15F-CC and 17F-CC. Bryozoans, pteropods, and bivalves were found in many samples in well-preserved condition. The overall assemblages suggest periodic variability between oxic and dysoxic conditions at this site.

Ostracods

Core catcher samples from Hole U1544A (18 samples) were also examined for the presence of ostracods. Ostracods were either absent or rare in most samples, except for Samples 383-U1544A-8H-CC and 19F-CC, where they were abundant (Table **T9**). The assemblage in these samples is composed of a mix of bathyal and shelf taxa, pointing to evidence of downslope transport of shelf deposits. However, time constraints prevented the tabulation of individual species counts.

Figure F19. Planktonic foraminifers, Site U1544. Scale bars = 100 µm. A. *Globigerina bulloides*. B. *Globigerinita glutinata*. C. *Neogloboquadrina incompta*. D. *Neogloboquadrina pachyderma*. E. *Orbulina universa*. F, G. *Truncorotalia crassaformis* in (F) umbilical and (G) side view. H, I. *Truncorotalia truncatulinoides* in (H) spiral and (I) umbilical view. J. *Hirsutella scitula*. K, L. *Globoconella inflata* in (K) side and (L) umbilical view.

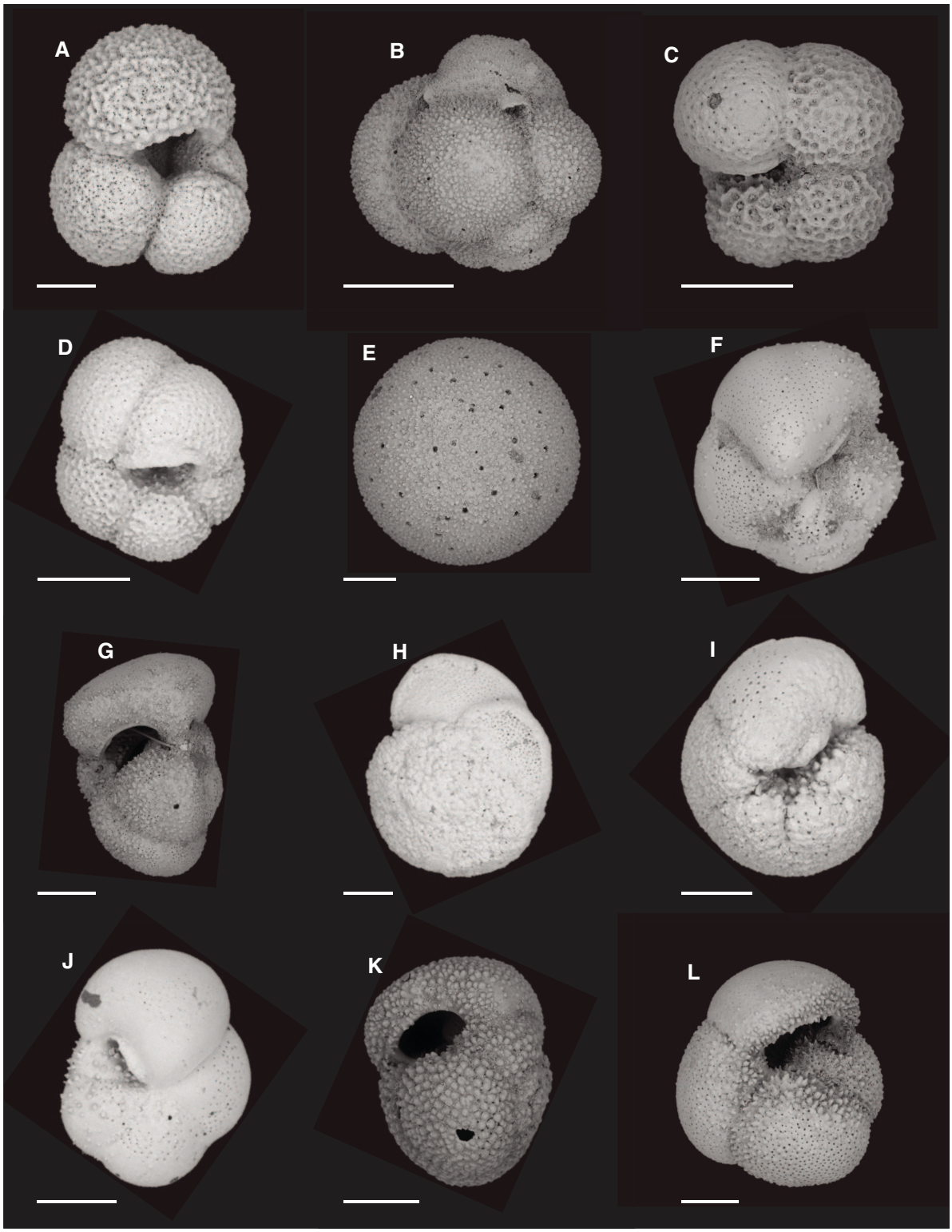

Table T8. Distribution chart of benthic foraminifers, Hole U1544A. **Download table in CSV format.**

Figure F20. Abundance of dominant benthic foraminifer genera and species *Uvigerina* spp., *Oridorsalis umbonatus*, *Melonis* spp., *Globocassidulina subglobosa*, *Cibicides*/*Cibicidoides* spp., *Fursenkoina* spp., and *Ehrenbergina* sp., Site U1544.

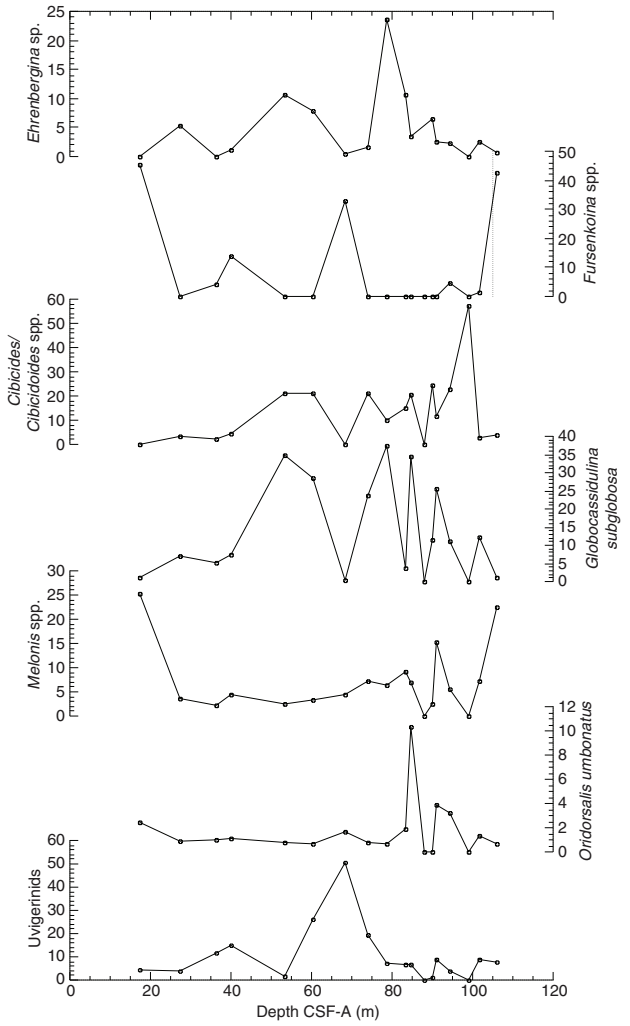

Table T9. Distribution chart of ostracods, Hole U1544A. **Download table in CSV format.**

Paleomagnetism

The natural remanent magnetization (NRM) of archive-half core sections from Site U1544 was measured and remeasured after alternating field (AF) demagnetization at 2 cm increments. In general, the number of demagnetization steps was selected based on the desire for more steps to study the magnetization(s), the severity of the drill string and natural overprints that hopefully can be removed to recover the natural remanence, the desire to use low-peak fields to preserve the magnetization for future shore-based studies, and the need to maintain core flow through the laboratory. For Hole U1544A, three (5, 10, and 15 mT) AF demagnetization steps were performed for the upper 40 m (through Section 383-U1544A-6H-4) to examine the drill string overprint and our ability to remove it. To keep up with core flow, the 5 mT step was removed and only the 10 and 15 mT steps were used for the rest of Hole U1544A. Data associated with intervals affected by obvious drilling disturbance or measurement error were culled prior to uploading or processing the

Figure F21. Natural remanent magnetization (NRM) intensities and inclination measured before and after 15 mT peak AF demagnetization, Hole U1544A.

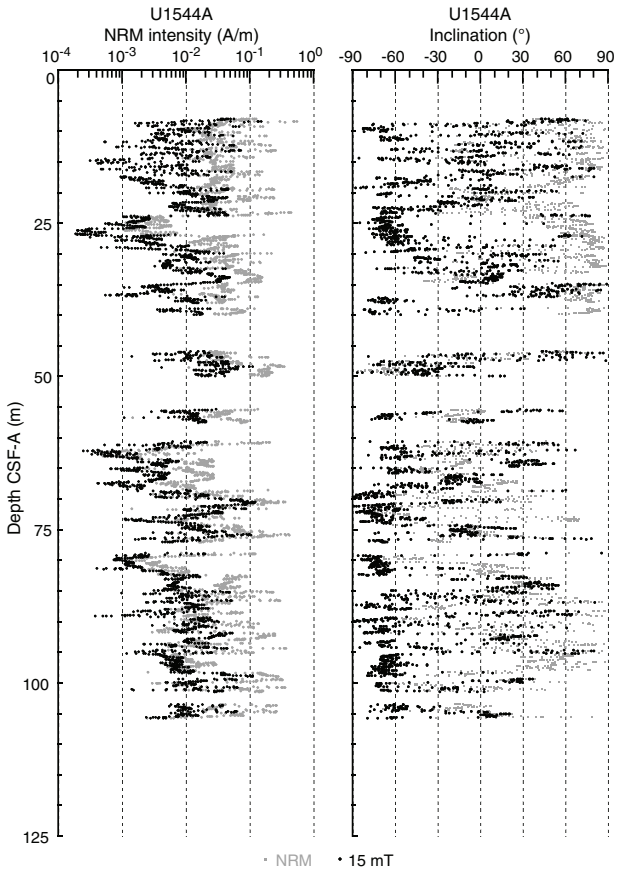

data. However, because of the nature of these sediments (see **Sedimentology**), it is challenging to confidently distinguish disturbed from pristine intervals. Therefore, sandy intervals and other intervals that do not preserve reliable NRMs remain in the record.

The intensities prior to demagnetization of cores recovered from Hole U1544A are relatively strong and generally lie in the 10^{-2} to 10^{-3} A/m range (Figure **F21**). Intensities drop slightly after demagnetization at a peak AF of 15 mT, consistent with removal of a drill string magnetic overprint. Inclinations both before and after AF demagnetization at 15 mT are quite variable, reflecting the sandy nature of these sediments. Fine-grained intervals are often better defined, and steep and positive inclinations prior to demagnetization and steep and negative inclinations after suggest removal of a drill string magnetic overprint giving way to a primary remanence that varies around expected directions (–71°) for the site latitude during normal polarity. Although the record is very noisy, no evidence for reliable reversed polarity is observed, suggesting that Site U1544 sediments are younger than 0.781 Ma (Hilgen et al., 2012).

Geochemistry

Sediment gas sampling

Routine safety hydrocarbon measurements were collected at Site U1544 in headspace gastight vials at a resolution of approximately one 5 cm^3 sample per core from 10.81 to 104.9 m CSF-A for

Hole U1544A (see **Geochemistry** in the Expedition 383 methods chapter [Winckler et al., 2021]). Methane concentrations increase from 32,830 ppmv at 10.81 m CSF-A to 60,311 ppmv at 47.17 m CSF-A and then decrease to 18,422 ppmv at 61.88 m CSF-A (Figure **F22**; see U1544-T1.xls in GEOCHEM in **Supplementary material**). Between 61.88 m CSF-A and the base of the core at 104.9 m CSF-A, methane does not exceed 38,495 ppmv. Methane concentrations are within safety limits (<200,000 ppmv) throughout Site U1544, according to the BBSCP Biogenic Methane Gas Safety Protocol. Ethane occurs at 47.17, 87.35, and 89.25 m CSF-A at relatively low concentrations of 0.73, 0.67, and 1.12 ppmv, respectively. Methane/ethane (C_1/C_2) ratios are 82,188 at 47.17 m CSF-A, 39,293 at 87.35 m CSF-A, and 38,505 at 89.25 m CSF-A. Propene occurs at a concentration of 0.48 ppmv at 89.25 m CSF-A, and ethene and propane remain below detection limit.

Interstitial water chemistry

At Site U1544, five whole rounds were collected for interstitial water (IW) samples from Hole U1544A at a resolution of one per core. Because the recovered sediment was soupy in nature and several core barrels were shattered, no whole rounds were taken below 72.740 m CSF-A. No mudline sample could be recovered. We squeezed whole rounds and subsampled for IW according to the methods described above (see **Geochemistry** in the Expedition 383 methods chapter [Winckler et al., 2021]).

Alkalinity and pH

Alkalinity decreases from 41 mM at 10.76 m CSF-A to 29 mM at 72.74 m CSF-A (Figure **F23**; see U1544-T2.xls in GEOCHEM in **Supplementary material**). pH varies between 7.83 and 7.93, and the range of values is too small and the sampling resolution too low to interpret any trends in pH with depth.

Salinity, chlorinity, and sodium

Salinity for all IW samples is between 34 and 35. At most depths, chloride concentrations vary between 550 and 558 mM (Figure **F24**). One high value of 600 mM occurs at 47.12 m CSF-A. Sodium is constant throughout the hole at an average of 458 ± 4 mM.

Ammonium, phosphate, and sulfate

Ammonium (NH_4^+) concentrations at this site generally increase with depth from 4744 µM at 10.76 m CSF-A to 6283 µM at 72.74 m CSF-A (Figure **F25**). Because these concentrations were unexpectedly high, these values fell outside the range of the calibration curve, and because of time constraints they could not be rerun. Thus, the absolute NH_4^+ values should be interpreted with care; however, the downhole trend is likely real. Phosphate (PO_4^{3-}) concentrations average 116.4 ± 1.5 µM (±1σ) with the exception of one low value of 91.2 µM at 47.12 m CSF-A. The relatively high NH_4^+ and PO_4^{3-} concentrations are likely related to organic matter degradation.

Sulfate (SO_4^{2-}) concentrations are extremely low, varying around an average of 0.13 mM ± 0.11 mM. Given the high methane concentrations, it is likely that all samples collected in this core were below the sulfate–methane transition zone (SMTZ), where SO_4^{2-} is completely consumed by the oxidation of upward-diffusing methane (Iverson et al., 1985).

Magnesium, calcium, and strontium

Magnesium (Mg) concentrations decrease slightly with depth from 50.5 mM at 10.76 m CSF-A to 44.3 mM at 72.74 m CSF-A (Figure **F26**). Calcium (Ca) and strontium (Sr) concentrations average 2.1 ± 0.7 mM and 74.8 ± 2.8 µM, respectively. The Ca and Sr profiles have similar shapes, which may reflect the fact that both are influenced by carbonate ($CaCO_3$) mineral dissolution and precipitation. However, as mentioned previously, the low sampling resolution makes interpreting downhole trends difficult.

Figure F22. Headspace methane concentrations, Site U1544.

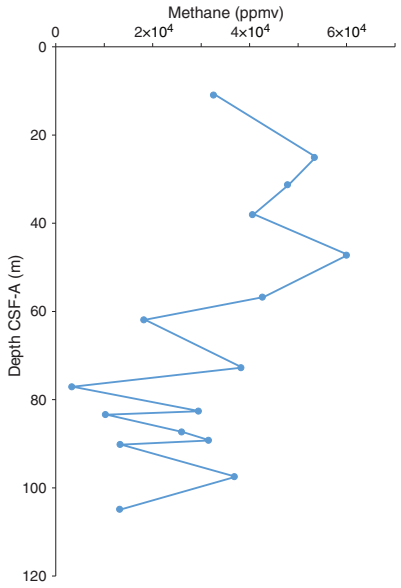

Figure F23. Interstitial water alkalinity and pH, Hole U1544A.

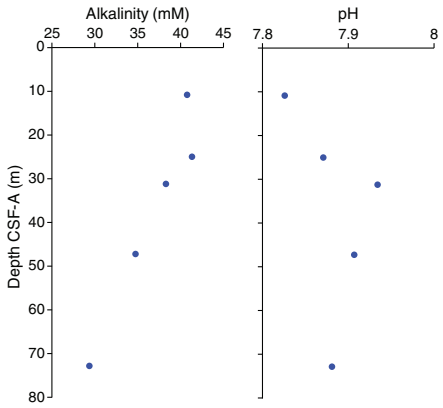

Figure F24. Interstitial water chloride and sodium, Hole U1544A.

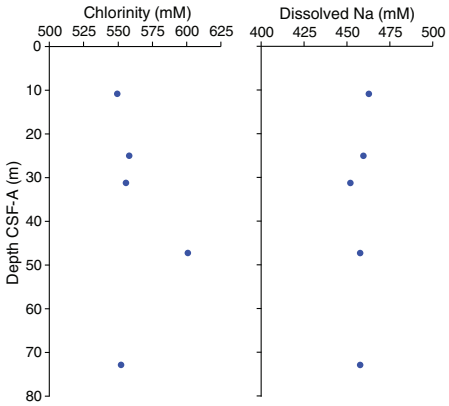

Figure F25. Interstitial water ammonium, phosphate, and sulfate, Hole U1544A.

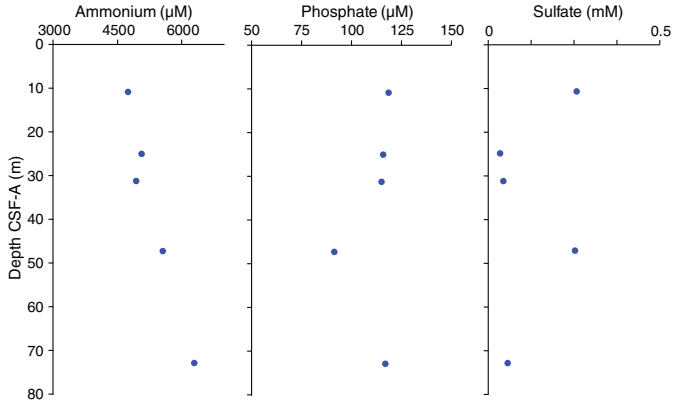

Figure F26. Interstitial water calcium, strontium, and magnesium, Hole U1544A.

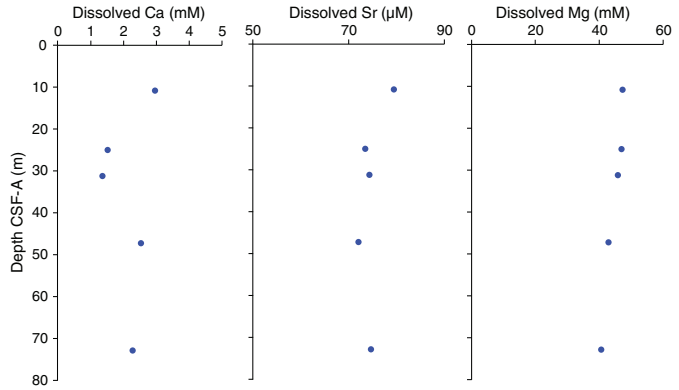

Iron, manganese, and lithium

Dissolved iron (Fe) concentrations are relatively high, ranging from 35.2 μM at 10.76 m CSF-A to 10.5 μM at 47.12 m CSF-A (Figure **F27**). At this site, Fe is likely released to the IW by microbial and/or abiotic Fe reduction and remains in solution because of an absence of sulfide below the SMTZ. In contrast to Fe, aqueous manganese (Mn) concentrations are relatively low, varying between 4.7 and 1.5 μM. Lithium (Li) exhibits a slight increase from 19.1 at 10.76 m CSF-A to 25.1 at 72.74 m CSF-A.

Silicon, barium, potassium, and bromide

Silicon (Si) concentrations are relatively variable at this site, averaging 687 ± 43 μM. They are likely controlled by dissolution of clay minerals and biogenic silica (Figure **F28**). Barium (Ba) concentrations are relatively high (average = 136 ± 27 μM), perhaps due to dissolution of barite ($BaSO_4$) in the absence of SO_4^{2-}. Potassium (K) and bromide (Br) show little variation downhole, averaging 10.8 ± 0.3 μM and 1.01 ± 0.05 μM, respectively. Depth trends in these elements cannot be reasonably interpreted because of the low sampling resolution.

Figure F27. Interstitial water iron, manganese, and lithium, Hole U1544A.

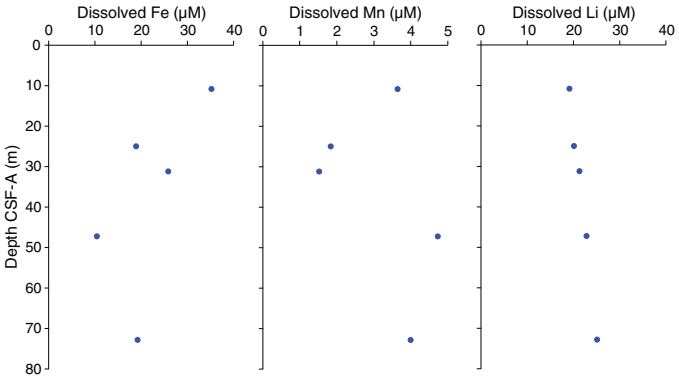

Bulk sediment

Total carbon and total nitrogen

Because of time limitations, only two individual samples in Sections 383-U1544A-4H-2 and 4H-6 were analyzed for total carbon (TC) and total nitrogen (TN). No $CaCO_3$ analyses were conducted at Site U1544. TC concentrations are 0.5 wt% at 19.06 m CSF-A and 7.4 wt% at 26.13 m CSF-A (see U1544-T3.xls in GEOCHEM in **Supplementary material**). Even without a direct carbonate measurement, these analyses suggest very low carbonate content for this site. TN concentrations are 0.07 wt% at 19.06 m CSF-A and 0.05 wt% at 26.13 m CSF-A, which are notably among the highest values observed during Expedition 383 and suggest a relatively high concentration of organic matter in the sampled intervals.

Bulk sediment inductively coupled plasma–atomic emission spectroscopy (ICP-AES) analyses could not be conducted because of time limitations.

Summary

The low sampling resolution makes it difficult to interpret IW profiles from this site. Low SO_4^{2-} and high methane concentrations suggest that the SMTZ occurs above ~10 m CSF-A (Iverson et al., 1985). The high alkalinity indicates that organic matter degradation is dominated by anaerobic processes, and concentrations of IW Fe suggest that microbial Fe reduction also occurs at this site.

Because of limited time, only two samples were analyzed for TN and TC, and observed TN values are among the highest among all Expedition 383 sites.

Figure F28. Interstitial water silicon, barium, potassium, and bromide, Hole U1544A.

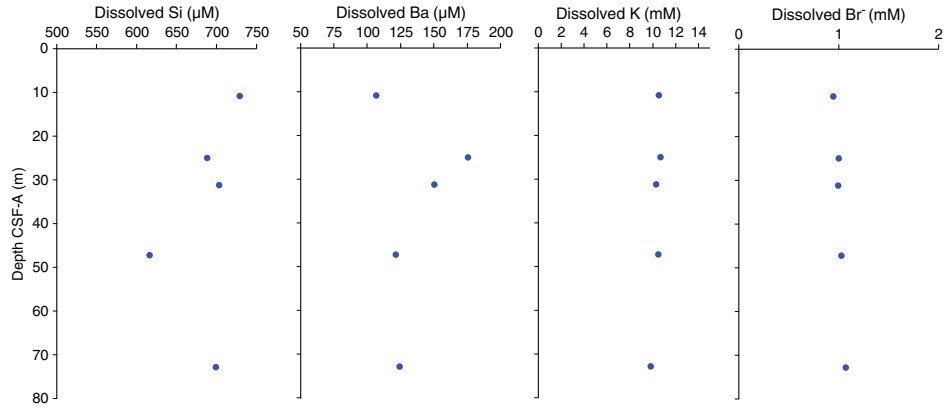

Physical properties

Shipboard physical properties measured at Site U1544 comprise nondestructive whole-round measurements of GRA bulk density and MS using the Whole-Round Multisensor Logger (WRMSL) and NGR measurements on cores from Hole U1544A. Cores 383-U1544A-1H through 4H were passed through the WRMSL and natural gamma radiation logger (NGRL) without temperature equilibration and then split. However, the remaining cores (5H–20F) were allowed to equilibrate to 17°C before measuring them at a 2 cm resolution on the WRMSL. For NGR, we kept the 10 cm resolution but used a lower 200 s integration time to facilitate faster processing at this shallower continental margin site.

No thermal conductivity or *P*-wave velocity measurements were taken at this site because the sections of unconsolidated sandy and silty material had a high water content and were expanding, rendering the measurements not representative of the sediments and unreliable. Five discrete moisture and density (MAD) samples were taken from the first APC core retrieved (383-U1544A-3H) before time constraints due to the upcoming port call prevented more MAD sampling. Archive halves were measured with the Section Half Multisensor Logger (SHMSL) for MS and color reflectance (see **Sedimentology**). Physical property data were analyzed for trends and variability, but the lack of a mudline core, coring gaps, fluid sands, and the presence of turbidites (see **Sedimentology**) made it challenging to correlate the records to other sites occupied during Expedition 383 or to late Pleistocene climate stages.

Magnetic susceptibility

Whole-round measurements on the WRMSL and discrete point measurements on the SHMSL were used to characterize the MS at Site U1544 (Figure **F29**). Both methods yielded a similar range of values and similar downhole variability.

Overall, most MS values range from ~25 to ~1550 instrument units (IU) (see **Physical properties** in the Expedition 383 methods chapter [Winckler et al., 2021] for details on instrument units [$\sim 10^{-5}$ SI]) for the WRMSL and SHMSL. A number of maxima comprising multiple data points exceeded this range and probably correspond to some of the dropstones found while sampling (Figure **F29**). Maxima in the MS record seem to correspond to cold phases, whereas the warmer intervals interpreted to occur from 23.3 to 26.45 m CSF-A, probably from 61.8 to 67.7 m CSF-A, and around 80 m CSF-A, based on planktonic microfossils and lithofacies (see **Biostratigraphy** and **Sedimentology**), correspond to the lowest MS values.

Figure F29. Whole-Round Multisensor Logger magnetic susceptibility (MS; red) and Section Half Multisensor Logger point magnetic susceptibility (MSP; orange), Hole U1544A.

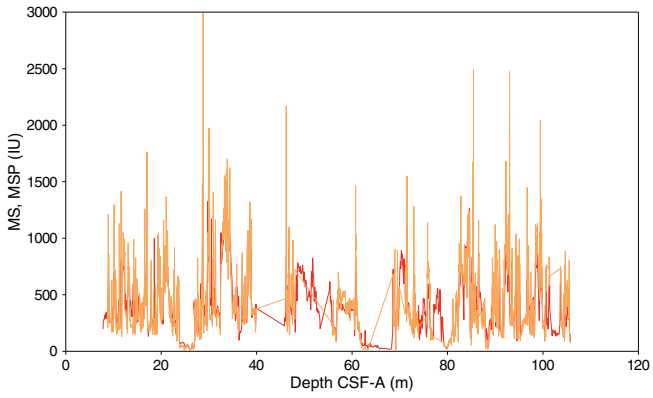

Figure F30. Splice data: WRMSL MS (red line), Section Half Multisensor Logger point magnetic susceptibility (MSP; orange), and gamma ray attenuation density–normalized natural gamma radiation (NGR*; black), Site U1544.

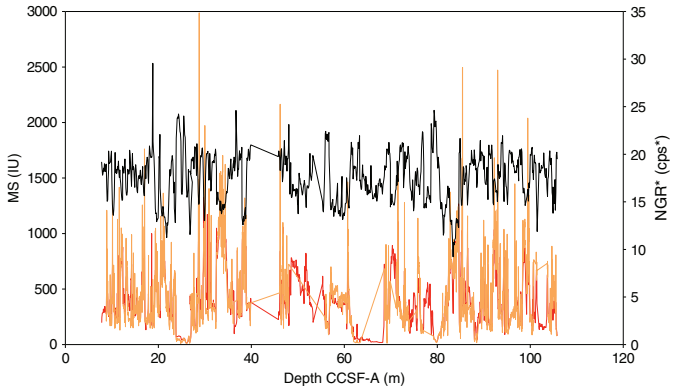

Natural gamma radiation

Density-normalized NGR measurements (NGR*) show downhole variations between about 9 to 30 counts/s (Figure **F30**). Similar to shallow Chilean margin Site U1542 (1100 meters below sea level [mbsl]), NGR is mainly anticorrelated with MS at Site U1544, indicating changes in the source and/or grain size composition of the terrigenous sediment fraction. The two intervals containing a higher abundance of

Figure F31. Calculated U/Th ratio from deconvolved gamma ray attenuation density–normalized natural gamma radiation (NGR*; blue) and NGR* (brown), Site U1544.

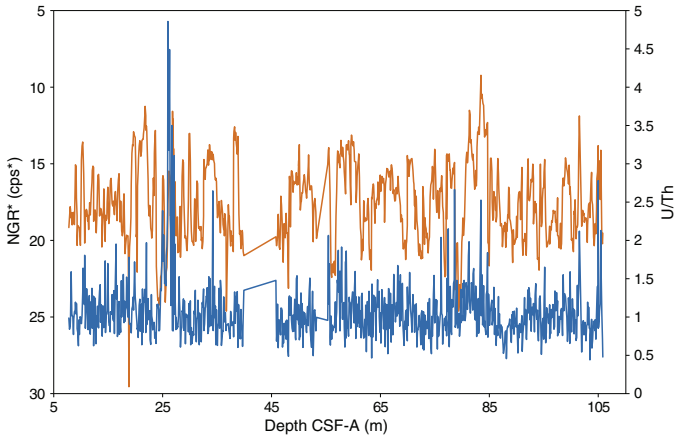

Figure F32. Bulk density from Whole-Round Multisensor Logger gamma ray attenuation (blue) and discrete moisture and density measurements (red), Site U1544.

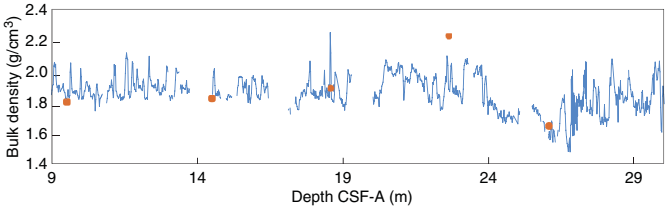

biogenic components correspond to high NGR* values, whereas the lowest values correspond to the sandy layers, which suggests a dominant grain size control of NGR* at this site (e.g., 75–79 m CSF-A).

In addition, we deconvolved the Site U1544 NGR counts into (semi)quantitative concentrations for the elements K, Th, and U following the methods of Dunlea et al. (2013) and De Vleeschouwer et al. (2017). In Figure **F31**, reversed NGR data are compared with the U/Th record. A clear peak in U/Th corresponds to the first high biogenic content interval (23.3–26.45 m CSF-A), and a bulge of higher U/Th corresponds to the second peak at ~80 m CSF-A.

Bulk density, grain density, and porosity

At Site U1544, we used GRA measurements at 2 cm spacing for Hole U1544A and five discrete MAD samples to evaluate changes in bulk density. Overall, GRA bulk density values from Hole U1544A vary mostly from ~1.2 to ~2.2 g/cm^3 and discrete MAD values range from ~1.6 to ~2.2 g/cm^3 (Figure **F32**). Low GRA values correspond to the higher biogenic content. The terrigenous material is associated with a variable amount of water, and sandy layers are represented both by high and low values in the GRA record (Figure **F32**) (see **Sedimentology**).

Summary

At Site U1544, the downhole changes in physical property characteristics do not show obvious features aligned with the defined lithofacies based on sedimentologic characteristics. Principally, lower MS and low GRA values match sediment intervals with higher contents of biogenic components, but they do not show a unique relationship with one another throughout the record (Figure **F33**). Comparing NGR and MS records could provide indications about the different terrigenous components because they are mainly anticorrelated, as at shallow-water Site U1542.

Figure F33. Processed Whole-Round Multisensor Logger (WRMSL) gamma ray attenuation bulk density (green) and WRMSL magnetic susceptibility (MS; red), Site U1544.

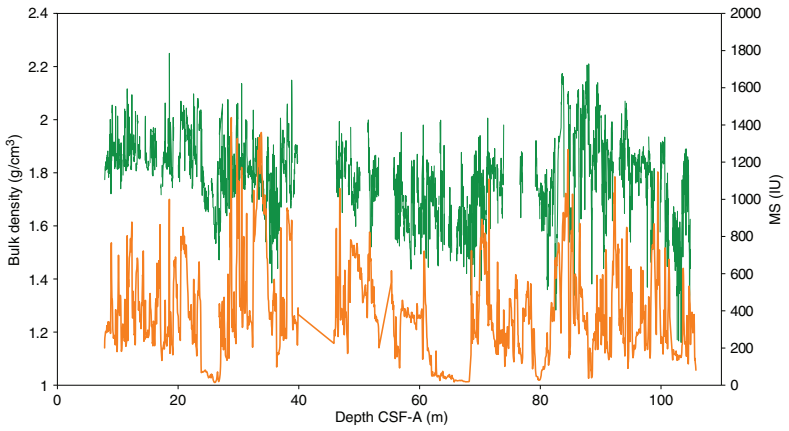

Stratigraphic correlation

Drilling at Site U1544 was terminated because of weather before a second hole could be initiated. As a result, there is no splice and no core composite depth below seafloor, Method A (CCSF-A), scale for Site U1544. All CSF-A depth scales for Site U1544 refer to Hole U1544A. Stratigraphic records from Hole U1544A should be interpreted with caution because stratigraphic gaps in sediment recovery likely occur between each core.

References

Boisvert, W.E., 1969. *Technical Report: Major Currents off the West Coasts of North and South America:* Washington, D.C. (Naval Oceanographic Office). **https://catalog.hathitrust.org/Record/008348460**

Bremer, M.L., and Lohmann, G.P., 1982. Evidence for primary control of the distribution of certain Atlantic Ocean benthic foraminifera by degree of carbonate saturation. *Deep-Sea Research, Part A: Oceanographic Research Papers*, 29(8):987–998. **https://doi.org/10.1016/0198-0149(82)90022-X**

Chaigneau, A., and Pizarro, O., 2005. Surface circulation and fronts of the South Pacific Ocean, east of 120°W. *Geophysical Research Letters,* 32(8):L08605. **https://doi.org/10.1029/2004GL022070**

De Vleeschouwer, D., Dunlea, A.G., Auer, G., Anderson, C.H., Brumsack, H., de Loach, A., Gurnis, M., et al., 2017. Quantifying K, U, and Th contents of marine sediments using shipboard natural gamma radiation spectra measured on DV *JOIDES Resolution*. *Geochemistry, Geophysics, Geosystems,* 18(3):1053–1064. **https://doi.org/10.1002/2016GC006715**

Dunlea, A.G., Murray, R.W., Harris, R.N., Vasiliev, M.A., Evans, H., Spivack, A.J., and D'Hondt, S., 2013. Assessment and use of NGR instrumentation on the *JOIDES Resolution* to quantify U, Th, and K concentrations in marine sediment. *Scientific Drilling,* 15:57–63. **https://doi.org/10.2204/iodp.sd.15.05.2013**

Fontanier, C., Jorissen, F.J., Chaillou, G., David, C., Anschutz, P., and Lafon, V., 2003. Seasonal and interannual variability of benthic foraminiferal faunas at 550 m depth in the Bay of Biscay. *Deep-Sea Research, Part I: Oceanographic Research Papers,* 50(4):457–494. **https://doi.org/10.1016/S0967-0637(02)00167-X**

Hilgen, F.J., Lourens, L.J., and Van Dam, J.A., 2012. The Neogene period. With contributions by A.G. Beu, A.F. Boyes, R.A. Cooper, W. Krijgsman, J.G. Ogg, W.E. Piller, and D.S. Wilson. *In* Gradstein, F.M., Ogg, J.G., Schmitz, M.D., and Ogg, G.M. (Eds.), *The Geologic Time Scale:* Oxford, United Kingdom (Elsevier), 923–978. **https://doi.org/10.1016/B978-0-444-59425-9.00029-9**

Hornibrook, N.d.B., 1981. *Globorotalia* (planktic Foraminiferida) in the late Pliocene and early Pleistocene of New Zealand. *New Zealand Journal of Geology and Geophysics,* 24(2):263–292. **https://doi.org/10.1080/00288306.1981.10422717**

Hornibrook, N.d.B., and Jenkins, D.G., 1994. DSDP 594, Chatham Rise, New Zealand—late Neogene planktonic foraminiferal biostratigraphy revisited. *Journal of Micropalaeontology,* 13(2):93–101. **https://doi.org/10.1144/jm.13.2.93**

Jenkins, D.G., 1993. Cenozoic southern mid- and high-latitude biostratigraphy and chronostratigraphy based on planktonic foraminifera. *In* Kennett, J.P., and Warnke, D.A. (Eds.), *The Antarctic Paleoenvironment: A Perspective on Global Change: Part Two.* Antarctic Research Series, 60:125–144. **https://agupubs.onlinelibrary.wiley.com/doi/abs/10.1002/9781118668061.ch7**

Jutzeler, M., White, J.D.L., Talling, P.J., McCanta, M., Morgan, S., Le Friant, A., and Ishizuka, O., 2014. Coring disturbances in IODP piston cores with implications for offshore record of volcanic events and the Missoula megafloods. *Geochemistry, Geophysics, Geosystems,* 15(9):3572–3590. **https://doi.org/10.1002/2014GC005447**

Lamy, F., 2016. The Expedition PS97 of the Research Vessel *POLARSTERN* to the Drake Passage in 2016. *Berichte zur Polar und Meeresforschung,* 701. **http://epic.awi.de/41674**

Lamy, F., Arz, H.W., Kilian, R., Lange, C.B., Lembke-Jene, L., Wengler, M., Kaiser, J., et al., 2015. Glacial reduction and millennial-scale variations in Drake Passage throughflow. *Proceedings of the National Academy of Sciences of the United States of America*, 112(44):13496–13501. **https://doi.org/10.1073/pnas.1509203112**

Lamy, F., Winckler, G., Alvarez Zarikian, C.A., and the Expedition 383 Scientists, 2021. Supplementary material, **https://doi.org/10.14379/iodp.proc.383supp.2021**. *Supplement to* Lamy, F., Winckler, G., Alvarez Zarikian, C.A., and the Expedition 383 Scientists, *Dynamics of the Pacific Antarctic Circumpolar Current.* Proceedings of the International Ocean Discovery Program, 383: College Station, TX (International Ocean Discovery Program). https://doi.org/10.14379/iodp.proc.383.2021

Murray, J.W., 1991. Ecology and distribution. *In* Takayanagi, Y., and Saito, T., (Eds.), *Studies in Benthic Foraminifera: Proceedings of the Fourth International Symposiyum on Benthic Foraminifera, Sendai, 1990:* Sendai, Japan (Tokai University Press).

Polonia, A., Torelli, L., Brancolini, G., and Loreto, M.-F., 2007. Tectonic accretion versus erosion along the southern Chile Trench: oblique subduction and margin segmentation. *Tectonics,* 26(3):TC1983. **https://doi.org/10.1029/2006TC001983**

Scott, G.H., Kennett, J.P., Wilson, K.J., and Hayward, B.W., 2007. *Globorotalia puncticulata*: population divergence, dispersal and extinction related to Pliocene–Quaternary water masses. *Marine Micropaleontology*, 62(4):235–253. **https://doi.org/10.1016/j.marmicro.2006.08.007**

Singh, R.K., and Gupta, A.K., 2010. Deep-sea benthic foraminiferal changes in the eastern Indian Ocean (ODP Hole 757B): their links to deep Indonesian (Pacific) flow and high latitude glaciation during the Neogene. *Episodes*, 33(2):74–82. **https://doi.org/10.18814/epiiugs/2010/v33i2/001**

Wei, K.-Y., 1994. Stratophenetic tracing of phylogeny using SIMCA pattern recognition technique: a case study of the late Neogene planktonic foraminifera *Globoconella* clade. *Paleobiology*, 20(1):52–65. **https://doi.org/10.1017/S0094837300011131**

Well, R., and Roether, W., 2003. Neon distribution in South Atlantic and South Pacific waters. *Deep-Sea Research, Part I: Oceanographic Research Papers*, 50(6):721–735. **https://doi.org/10.1016/S0967-0637(03)00058-X**

Winckler, G., Lamy, F., Alvarez Zarikian, C.A., Arz, H.W., Basak, C., Brombacher, A., Esper, O.M., Farmer, J.R., Gottschalk, J., Herbert, L.C., Iwasaki, S., Lawson, V.J., Lembke-Jene, L., Lo, L., Malinverno, E., Michel, E., Middleton, J.L., Moretti, S., Moy, C.M., Ravelo, A.C., Riesselman, C.R., Saavedra-Pellitero, M., Seo, I., Singh, R.K., Smith, R.A., Souza, A.L., Stoner, J.S., Venancio, I.M., Wan, S., Zhao, X., and Foucher McColl, N., 2021. Expedition 383 methods. *In* Lamy, F., Winckler, G., Alvarez Zarikian, C.A., and the Expedition 383 Scientists, *Dynamics of the Pacific Antarctic Circumpolar Current.* Proceedings of the International Ocean Discovery Program, 383: College Station, TX (International Ocean Discovery Program). **https://doi.org/10.14379/iodp.proc.383.102.2021**

Zielinski, U., and Gersonde, R., 2002. Plio–Pleistocene diatom biostratigraphy from ODP Leg 177, Atlantic sector of the Southern Ocean. *Marine Micropaleontology,* 45(3–4):225–268. **https://doi.org/10.1016/S0377-8398(02)00031-2**